**Biogeosciences
Discussions**

The value of adding optics to ecosystem models: a case study

M. Fujii[1,*], E. Boss[1], and F. Chai[1]

[1]School of Marine Sciences, 5706 Aubert Hall, University of Maine, Orono, ME 04469-5706, USA
[*]now at: Sustainability Governance Project, Creative Research Initiative "Sousei", Hokkaido University, N9W8, Kita-ku, Sapporo, Hokkaido 060-0809, Japan

Correspondence to: M. Fujii (mfujii@sgp.hokudai.ac.jp)

BGD

4, 1585–1631, 2007

Bio-optical modeling

M. Fujii et al.

Title Page

Abstract | Introduction

Conclusions | References

Tables | Figures

|◄ | ►|

◄ | ►

Back | Close

Full Screen / Esc

Printer-friendly Version

Interactive Discussion

EGU

Abstract

Many ecosystem models have been developed to study the ocean's biogeochemistry, but most of these models use simple formulations to describe light penetration and spectral quality. Given that processes such as photosynthesis and photo-oxidation are
5 uniquely important for biogeochemical processes in the upper ocean, it is necessary to model light distribution accurately. In addition, the global scale observations of proxies of biogeochemical variables are based on the color of the ocean. The ability to simulate the color of the ocean provides the possibility of comparing model simulation with these observations. Here, an optical model is coupled with a previously published ecosys-
10 tem model that explicitly represents two phytoplankton (picoplankton and diatoms) and two zooplankton functional groups, as well as multiple nutrients and detritus. Surface ocean color field and subsurface light field are calculated by coupling the ecosystem model with an optical model that relates biogeochemical standing stocks with inherent optical properties (absorption, scattering); this provides input to a commercially
15 available radiative transfer model (Ecolight). We apply this bio-optical model to the equatorial Pacific upwelling region, and find the model to be capable of reproducing many measured optical properties and key biogeochemical processes in this region. Results include large contributions by non-algal particles to the total scattering or attenuation (>50% at 660 nm) and their small contribution to particulate absorption (<20%
20 at 440 nm), and a remarkable contribution by picoplankton to total phytoplankton absorption (>95% at 440 nm). These results are consistent with the field observations. In order to achieve such good agreement between data and model results, however, key model parameters, for which no field data is available, have to be constrained. Sensitivity analysis of the model results to optical parameters reveals the significant role of
25 colored dissolved organic matter to the modeled properties. Coupling explicit optics to an ecosystem model provides several advantages in generating: (1) a more accurate subsurface light-field, which is important for light sensitive biogeochemical processes such as photosynthesis and photo-oxidation, (2) added constraints on model parame-

ters that help to reduce uncertainties in ecosystem model simulations, and (3) model output which is comparable to basic remotely-sensed properties. In addition, the coupling of biogeochemical models and optics paves the road for future assimilation of ocean color and in-situ measured optical properties into the models.

1 Introduction

Marine ecosystem models have increased their relevance by incorporating greatly enhanced spatial resolution and more sophisticated representations of functional groups (e.g. Rothstein et al., 2006). The models vary from the simplest nutrient/phytoplankton/zooplankton/detritus (NPZD) models (e.g. Riley et al., 1949; Denman and Peña, 2002; Schartau and Oschlies, 2003) to complex models with twenty or more components including different types of plankton, nutrients, and a microbial loop (e.g. Bissett et al., 1999; Moore et al., 2002; Gregg et al., 2003; Lancelot et al., 2005) accompanied with an increase in the number of specified parameters (e.g. Denman, 2003; Friedrichs et al., 2007).

Progress in ocean color remote sensing technology and inversion algorithms has provided ways to assess standing stocks of phytoplankton pigments and carbon (Behrenfeld et al., 2005), particulate organic carbon (POC, Stramski et al., 1999), and colored dissolved organic matter (CDOM, Siegel et al., 2002) through their unique scattering and/or absorption signatures. Global net oceanic primary productivity (carbon fixation) has been estimated with satellite data, based on derived surface chlorophyll concentration (e.g. Behrenfeld and Falkowski, 1997) and more recently from remote estimation of both phytoplankton carbon and chlorophyll (Behrenfeld et al., 2005). Many of these advances are based on semi-empirical algorithms linking ocean color to the optical properties of the underlying constituents (IOCCG, 2006).

Given the ability to measure optical properties from small, robust, and high-frequency sensors in-situ and on a variety of platforms (e.g. Rudnick and Perry, 2003), a large body of work has been assembled linking biogeochemical variables to optical proper-

EGU

ties (e.g. Dickey et al., 2006).

Considering this progress in observational capabilities, if we are to compare models to measurements and/or assimilate measurements into models, it is imperative to contemplate modeling not only the biogeochemical but also the inherent optical properties (IOP) such as absorption and backscattering as state variables, and to compare results directly to estimates from remotely observed or in-situ measured quantities. Conversion of biogeochemical properties to optical parameters is also needed to model realistically the underwater light field, which is used as input to calculate model processes such as photosynthesis and photochemistry. The optical consequences of seawater constituents, including dissolved materials, phytoplankton, and non-algal particles (NAP), need to be included in ecosystem models, and the interaction of light with these materials needs to be computed to obtain realistic depth- and wavelength-resolved light fields. However, with very few exceptions (e.g. Bissett et al., 1999), most ecosystem models do not include the physics and bio-optics associated with the underwater light field. In addition, Rothstein et al. (2006) have recently reviewed the state of the art of modeling harmful algal blooms and specifically recommended the development of ecosystem models which includes optics.

In this study, we develop a multi-nutrient phytoplankton, zooplankton, and detritus ecosystem model with associated wavelength-resolved optical properties. We choose to simulate the equatorial Pacific where data from several programs are available. In the following section, the various components of the ecosystem model and the simulation design are described. Section 3 outlines and discusses the results of this modeling study and a model sensitivity analysis to optical parameters. These results highlight the fact that the bio-optical model reproduces well the measured biogeochemical and optical features, and that optical properties play an important role in identifying and reducing uncertainties in ecosystem models, providing constraints for determining variables and related parameters. A summary is presented in Sect. 4.

EGU

2 Model description and experimental design

The bio-optical model constructed in this study consists of four individual models: a physical-ecosystem model (simulating the dynamics of different ecosystem components in time and space), a photo-acclimation model (specifying the chlorophyll to carbon ratio of phytoplankton), an optical model (converting ecosystem state variables into inherent optical properties), and a radiative transfer model (calculating the underwater light field and the ocean color; Fig. 1). For the sake of simplicity and ease of comparison with data, we demonstrate area-averaged one dimensional (vertical) and time-averaged results. The model, however, is formulated and designed to be used in 4 dimensions.

2.1 Physical-ecosystem model and photo-acclimation model

The physical-ecosystem model used in this study is based on the Carbon, Silicon, Nitrogen Ecosystem (CoSINE) model (Chai et al., 2002), which was developed originally to simulate biogeochemistry in the equatorial Pacific upwelling region. The ecosystem model explicitly represents two phytoplankton (picoplantkon P1 ($mmolN\,m^{-3}$) and diatoms P2 ($mmolN\,m^{-3}$)) and two zooplankton functional groups (microzooplankton Z1 ($mmol\,Nm^{-3}$) and mesozooplantkon Z2 ($mmolN\,m^{-3}$)), as well as multiple nutrients (nitrate NO_3 ($mmolN\,m^{-3}$), ammonium NH_4 ($mmolN\,m^{-3}$), and silicate $Si(OH)_4$ ($mmolSi\,m^{-3}$)) and detritus (non-algal particles NAP ($mmolN\,m^{-3}$) and biogenic silica $bSiO_2$ ($mmolSi\,m^{-3}$)) (Fig. 2). Phytoplankton take up NO_3 and NH_4 by photosynthesis. In addition, diatoms utilize $Si(OH)_4$ in the silicification process. Microzooplankton graze on picoplankton. Mesozooplankton feed on diatoms, microzooplankton, and NAP.

To reproduce observed variation in phytoplanktonic chlorophyll to carbon ratio with growth conditions (light, nutrients, and temperature), we incorporated a photo-acclimation model into the physical-ecosystem model. Geider et al. (1987, 1998) developed a photo-acclimation model with single nutrient (nitrogen) and single phytoplankton species. The photo-acclimation model used here is based on that of Moore

EGU

et al. (2002)'s study which modified the Geider et al. (1998)'s photo-acclimation model so that it could be embedded in the multi-nutrient, phytoplankton, zooplankton, and detritus ecosystem model.

The governing equations and formulations of physical-ecosystem model and photo-acclimation model are described in Appendix A. The biogeochemical parameter values used in this study and their notations are provided in Table 1.

2.2 Optical model and radiative transfer model

We developed an optical module that explicitly represents spectrally-resolved inherent optical properties (IOPs, e.g. absorption, scattering, and attenuation) from the ecosystem model variables. Using a radiative-transfer model, we obtain the apparent optical properties (AOPs), such as diffuse attenuation, and radiometric quantities, such as photosynthetically available radiation (PAR) and remotely sensed reflectance (ocean color).

The absorption coefficient is determined from the sum of the absorption coefficients of seawater, picoplankton and diatoms (based on their chlorophyll content, Chl1 and Chl2, respectively), non-algal particles (NAP), and colored dissolved organic matter (CDOM). Notable differences exist in the chlorophyll-specific absorption coefficient ($m^2 mg^{-1}$) of small and large phytoplankton, i.e. small phytoplankton have a higher chlorophyll-specific absorption coefficient and a steeper absorption spectra than large phytoplankton. In addition, the absorption spectra of a given phytoplankton functional group changes with intercellular chlorophyll concentration (the package effect, e.g. Duysens, 1956). Therefore, the chlorophyll-specific absorption coefficients by picoplankton and diatoms, $a_{\phi 1}^{*}$ and $a_{\phi 2,}^{*}$ are modeled separately, taking into account their photo-adaptive state (e.g. their specific chlorophyll to carbon ratio) as follows (Fig. 3b):

$$a_{\phi 1}^{*}(\lambda, z)(m^2\,mg^{-1}) = a_{\phi 1(\text{high light})}^{*}(\lambda) \times (1 - \frac{\frac{Chl1(z)}{C1(z)} - \theta_{\min}^{C}}{\theta_{\max}^{C} - \theta_{\min}^{C}}) + a_{\phi 1(\text{low light})}^{*}(\lambda) \times \frac{\frac{Chl1(z)}{C1(z)} - \theta_{\min}^{C}}{\theta_{\max}^{C} - \theta_{\min}^{C}}, \quad (1)$$

Bio-optical modeling

M. Fujii et al.

Title Page

Abstract	Introduction
Conclusions	References
Tables	Figures

◀◀   ▶▶

◀   ▶

Back   Close

Full Screen / Esc

Printer-friendly Version

Interactive Discussion

EGU

$$a^*_{\phi 2}(\lambda, z)(\text{m}^2\,\text{mg}^{-1}) = a^*_{\phi 2(\text{high light})}(\lambda) \times (1 - \frac{\frac{Chl2(z)}{C2(z)} - \theta^C_{min}}{\theta^C_{max} - \theta^C_{min}}) + a^*_{\phi 2(\text{low light})}(\lambda) \times \frac{\frac{Chl2(z)}{C2(z)} - \theta^C_{min}}{\theta^C_{max} - \theta^C_{min}}, \quad (2)$$

where $a^*_{\phi 1(\text{high light})}(\lambda)$, $a^*_{\phi 1(\text{low light})}(\lambda)$, $a^*_{\phi 2(\text{high light})}(\lambda)$, and $a^*_{\phi 2(\text{low light})}(\lambda)$ are chlorophyll-specific absorption coefficients at low and high light by each phytoplankton, respectively, derived as described in Appendix B. θ^C_{min} and θ^C_{max} are the minimum and maximum phytoplanktonic chlorophyll to carbon ratios which are set to be 0.036 (mgChl mmolC^{-1}) and 1.2 (mgChl mmolC^{-1}), respectively, based on measurements in phytoplankton cultures (e.g. Falkowski et al., 1985; Geider et al., 1987; Cloern et al., 1995). The absorption coefficient by total phytoplankton a_ϕ is:

$$a_\phi(\lambda, z)(m^{-1}) = a^*_{\phi 1}(\lambda, z) \times \text{Chl1}(z) + a^*_{\phi 2}(\lambda, z) \times \text{Chl2}(z). \quad (3)$$

Based on observations (e.g. Iturriaga and Siegel, 1989; Roesler et al., 1989), the absorption coefficient by NAP (a_{NAP}) is formulated as:

$$a_{\text{NAP}}(\lambda, z)(m^{-1}) = a^+_{\text{NAP}}(440) \times \text{NAP}(z) \times R_{CN} \times 12.0 \times 0.001 \times \exp\{-0.011 \times (\lambda - 440)\}, \quad (4)$$

where $a^+_{\text{NAP}}(440)$ is the carbon-specific absorption coefficient by NAP at 440 nm, assumed to be 0.1 (m^2 gC^{-1}) based on results of $a_{\text{NAP}}(440)$ / (dry mass) $\sim$0.036 $\pm$ 0.025 (m^{2}g^{-1}) (Babin et al., 2003b; Table 5), and using a conversion of 2.6 (g gC^{-1}) (Babin et al., 2003a). Note that modeled NAP is in nitrogen (mmol m^{-3}) and is converted to carbon unit (gC m^{-3}). R_{CN} is the ratio of carbon to nitrogen in phytoplankton (Table 1).

The total absorption coefficient by particles a_p is then calculated:

$$a_p(\lambda, z) = a_\phi(\lambda, z) + a_{\text{NAP}}(\lambda, z). \quad (5)$$

Although effects of dissolved material on absorption in equatorial regions cannot be neglected (e.g. Pegau, 1997; Bricaud et al., 2002; Simeon et al., 2003), information concerning the distribution of CDOM in the equatorial Pacific is scarce. In addition, ratios of CDOM to dissolved organic matter (DOM) or DOM to dissolved organic carbon

Bio-optical modeling

M. Fujii et al.

Title Page

Abstract | Introduction

Conclusions | References

Tables | Figures

|◄ | ►|

◄ | ►

Back | Close

Full Screen / Esc

Printer-friendly Version

Interactive Discussion

EGU

(DOC) are highly variable regionally (Mueller and Lange, 1989; Siegel et al., 2002). In this study, because CDOM is not explicitly treated in the model, the absorption coefficient by CDOM (a_{CDOM}) is assumed constant vertically and with a spectral dependence of (Fig. 3d):

$$a_{CDOM}(\lambda)(m^{-1}) = a_{CDOM}(440) \times \exp\{-0.0145 \times (\lambda - 440)\}, \tag{6}$$

where $a_{CDOM}(440)$ is the absorption coefficient of CDOM at 440 nm and the value is fixed to 0.016 (m^{-1}) in this study, following observational values in the equatorial Pacific (0.012–0.019; Simeon et al., 2003).

Although the observed ratios of backscattering to scattering by particles (b_{bp}/b_p) are relatively low (0.5–3%) (e.g. Twardowski et al., 2001), backscattering plays an important role in ocean optics in general, and especially in determining ocean color. Assuming no contribution of CDOM to backscattering (e.g. Stramski et al., 2004), backscattering coefficients by algae and the co-varying particles are expressed as a function of POC concentration of small and large particles (POC1 and POC2, respectively) (mg m^{-3}), which consist of algal and associated NAP related to small and large phytoplankton functional groups, respectively. Backscattering by small and large POC, b_{bp1} and b_{bp2}, are formulated as follows (based on Fig. 4b in Stramski et al., 1999):

$$b_{bp1}(\lambda, z)(m^{-1}) = \left(\frac{POC1(z)}{476\,935.8}\right)^{\frac{1}{1.277}} \times \left(\frac{\lambda}{510}\right)^{-0.5}, \tag{7}$$

$$b_{bp2}(\lambda, z)(m^{-1}) = \left(\frac{POC2(z)}{17\,069.0}\right)^{\frac{1}{0.859}}. \tag{8}$$

Backscattering by total particles b_{bp} is expressed:

$$b_{bp}(\lambda, z)(m^{-1}) = b_{bp1}(\lambda, z) + b_{bp2}(\lambda, z) + b_{bbg}, \tag{9}$$

where b_{bbg} is the background backscattering coefficient that implicitly reflects contribution by non-phytoplankton-covarying bacteria and other particles and was fixed to

Title Page

Abstract | Introduction

Conclusions | References

Tables | Figures

◄ | ►

◄ | ►

Back | Close

Full Screen / Esc

Printer-friendly Version

Interactive Discussion

EGU

0.00017 (m^{-1}), which is calculated using backscattering coefficients from Stramski and Kiefer (1991) and a field-based background heterotrophic bacterial concentration of 7×10^{11} (m^{-3}) from Cho and Azam (1990) (as in Behrenfeld and Boss, 2006).

Total scattering by particles b_p is calculated as follows:

$$b_p(\lambda, z) = R^{\phi}_{POC} \times \tilde{b}_{b\_P1} \times b_{bp1}(\lambda, z) + R^{\phi}_{POC} \times \tilde{b}_{b\_P2} \times b_{bp2}(\lambda, z)$$
$$+ (1 - R^{\phi}_{POC}) \times \tilde{b}_{b\_NAP} \times (b_{bp1}(\lambda, z) + b_{bp2}(\lambda, z)) + \tilde{b}_{b\_bg} \times b_{bbg}(\lambda, z),$$ (10)

where $\tilde{b}_{b\_P1}$, $\tilde{b}_{b\_P2}$, $\tilde{b}_{b\_NAP,}$ and $\tilde{b}_{b\_bg}$ are the backscattering ratios for picoplankton (0.01; based on near surface observations in open-ocean waters in Twardowski et al., 2001), diatoms (0.006; based on near-surface coastal observations in Twardowski et al., 2001, and Boss et al., 2004), NAP (0.015; e.g. Twardowski et al., 2001) and other background particles (0.02; e.g. Twardowski et al., 2001), respectively. Results from previous studies indicate that the ratio of phytoplankton carbon to POC (R^{ϕ}_{POC}) varies between about 25% and 40% in space and time (e.g. Eppley et al., 1992; DuRand et al., 2001; Gundersen et al., 2001; Oubelkheir et al., 2005). Considering these studies, we fix the ratio of picoplankton carbon to POC1 and diatom carbon to POC2 to 0.3.

Beam attenuation coefficient by particles c_p is expressed as follows:

$$c_p(\lambda, z)(m^{-1}) = a_p(\lambda, z) + b_p(\lambda, z).$$ (11)

Total absorption, scattering, and backscattering coefficients, a, b and b_b, are calculated

$$a(\lambda, z)(m^{-1}) = a_{sw}(\lambda) + a_p(\lambda, z) + a_{CDOM}(\lambda),$$ (12)

$$b(\lambda, z)(m^{-1}) = b_{sw}(\lambda) + b_p(\lambda, z),$$ (13)

$$b_b(\lambda, z)(m^{-1}) = \tilde{b}_{b\_sw} \times b_{sw}(\lambda) + b_{bp}(\lambda, z),$$ (14)

where a_{sw} and b_{sw} are absorption and backscattering coefficients by seawater, respectively. The coefficients depend on wavelengths and are obtained from Pope and Fry

Bio-optical modeling

M. Fujii et al.

⏮ | ⏭

◀ | ▶

Back | Close

Full Screen / Esc

Printer-friendly Version

Interactive Discussion

EGU

(1997) with the correction for salts (Morel, 1974; Boss and Pegau, 2001) (Figs. 3a and 4a). $\tilde{b}_{b\_sw}$ is the backscattering ratio for sea water (0.5; e.g. Morel, 1974).

The model-derived spectral absorption, a Fournier-Forand phase function with the model-derived particulate backscattering ratio (Fournier and Forand, 1994; Mobley et al., 2002), and sky and surface wave conditions, are all input into a radiative transfer model (Ecolight; Sequoia Scientific, Inc.) which calculates the underwater light field from which the downwelling photosynthetically available radiation (PAR) (W m^{-2}) is obtained and used as an input to light-sensitive processes in the ecosystem model. A semi-empirical sky model based on RADTRAN (Gregg and Carder, 1990), which is embedded in Ecolight, is used to calculate the hourly irradiance at the sea surface for the appropriate date and location, assuming no cloud cover and a surface wave field consistent with a daily-averaged wind speed of 5 m s^{-1}. See Mobley and Sundman (2005a, b) for details of Ecolight.

2.3 Experimental design

The physical-ecosystem simulation model, photo-acclimation model, optical model and radiative transfer model (Ecolight) are linked (Fig. 1) and applied to the equatorial Pacific upwelling region (5° S–5° N, 90°–180° W, the "Wyrtki Box"; Wyrtki, 1981). The physical forcing and most of the biogeochemical parameter values are the same as in Chai et al. (2002) (Table 1), although the photo-acclimation model was not introduced by Chai et al. (2002). Hourly incident sky radiance on 30 June, which represents well the annual-mean condition in this oceanic region, is used to drive Ecolight. The short time step of the model is needed to simulate diurnal cycles of biology, particularly for phytoplankton, because the photosynthesis is controlled by irradiance at each time step. We tested increasing the time step and found that it could be no longer than three hours before significant differences are observed. Shorter time steps did not change the simulation markedly and would represent an undesirable increase in computation load.

Next, steady-state results, obtained by running the model up to 1000 days with the

Full Screen / Esc

Printer-friendly Version

Interactive Discussion

EGU

area-averaged (5° S–5° N, 90° W–180°) annual-mean vertical velocity from the ocean general circulation model (Chai et al., 1996) and the area-averaged (5° S–5° N, 90° W–180°) annual-mean vertical diffusivity based upon the formulation by Pacanowski and Philander (1981) (Fig. 1 in Chai et al., 2002), are compared to measurements in the equatorial Pacific.

We set all the parameter values in the photo-acclimation model to the same as in previous studies (Geider et al., 1998; Moore et al., 2002) (Table 1). Most of the parameter values in the ecosystem model are set to the same as in Chai et al. (2002). Given that the maximum specific grazing rate by mesozooplankton ($G2_{max}$) has a relatively large uncertainty in the value, and the estimated value differs among previous studies with the same ecosystem model (Chai et al., 2002; Jiang et al., 2003; Fujii and Chai, 2007), we modify this parameter's value (tune it) so that the modeled surface nitrate and silicate concentrations would be the closest to the standard measurements in the equatorial Pacific of 6 (mmolN m^{-3}) and 3 (mmolN m^{-3}), respectively (Figs. 5b, d). In addition, the model results are examined to reproduce the following observations: (1) values and the types of decrease with depth for PAR and net community production (Figs. 5a, c); (2) maximal chlorophyll concentration of ca. 0.4 (mgChl m^{-3}) in the subsurface layer around 50 m depth; and (3) characteristically small NAP contribution to total particle absorption in the euphotic layer of 10–17% (Fig. 6b). The tuning is continued until all the observed bio-optical features in this region are reproduced by the model (see below).

3 Results and discussion

3.1 Biological properties

With the parameter values obtained by the procedure described in the previous subsection (Table 1), the tuned model is capable of reproducing well the measured vertical features in biogeochemistry in the equatorial Pacific upwelling region, i.e. consistently

Bio-optical modeling

M. Fujii et al.

Title Page

Abstract	Introduction
Conclusions	References
Tables	Figures

◀◀   ▶▶

◀   ▶

Back   Close

Full Screen / Esc

Printer-friendly Version

Interactive Discussion

EGU

higher NO_3 than $Si(OH)_4$ concentration and surface maximum in net community production (blue lines in Figs. 5b–d; e.g. Barber et al., 1996). The model also reproduces a subsurface chlorophyll maximum of 0.34 ($mgChl\,m^{-3}$) at around 65–70 m depth (blue line in Fig. 5e), which agrees with the observed maximal value of 0.4 ($mgChl\,m^{-3}$)

5 (Dupouy et al., 2003). The modeled phytoplanktonic chlorophyll to carbon ratio decreases with PAR, or increases exponentially with depth (Fig. 7), which also is consistent with observations (e.g. Chavez et al., 1991).

3.2 Optical properties

3.2.1 Absorption

10 Modeled absorption by phytoplankton at 440 nm ($a_\phi(440)$) has its subsurface maximum of 0.023 (m^{-1}) (Fig. 6a), which agrees well with observations (0.021±0.001, Simeon et al., 2003, and 0.023 (m^{-1}), Dupouy et al., 2003). The modeled absorption maximum appears at around 70–95 m depth, which is deeper than the chlorophyll maximum (blue line in Fig. 5e and Fig. 6a). This is because chlorophyll absorption is mostly contributed

15 by picoplankton (P1), which has its maximum chlorophyll at deeper layers than diatoms (P2) (Fig. 6a). Modeled contribution of picoplankton to phytoplankton absorption varies between 90 and 98% in the euphotic layer, which is consistent with the value of 97% reported for this region (Dupouy et al., 2003).

 Modeled absorption by NAP at 440 nm ($a_{NAP}(440)$) increases with depth and has a

20 maximum of 0.0035 (m^{-1}) (Fig. 6a). The vertical profile corresponds to that of NAP concentration (Fig. 5f) and the maximal value is consistent with a measured high value of 0.003 (m^{-1}) (Dupouy et al., 2003). The absorption by NAP is lower than that of picoplankton ($a_{\phi 1}(440)$) but is higher than that of diatoms ($a_{\phi 2}(440)$), indicating low but significant contribution of NAP to the total particulate absorption in the equatorial

25 Pacific (Fig. 6a). The modeled NAP contribution to total particle absorption reproduces the observed increase with depth, from 8% in the surface and up to 33% at the bottom of the euphotic layer (120 m depth) (Fig. 6b). The mean NAP contribution to total

EGU

particle absorption in the euphotic layer is 17%, which is consistent with measurements of 10–17% (Dupouy et al., 1997 and 2003; Parslow et al., 1998; Bricaud et al., 2002).

Colored dissolved organic matter (CDOM) also plays an important role in absorption (e.g. Pegau, 1997; Bricaud et al., 2002; Simeon et al., 2003). We fixed the absorption coefficient by CDOM at 440 nm ($a_{CDOM}(440)$) vertically to 0.016 (m^{-1}), within the observed range (0.012–0.019 (m^{-1}); Simeon et al., 2003). Modeled contribution of CDOM to total absorption at 440 nm ($a(440)$) is 59–97% and tends to increase with depth, consistent with measurements (50% at surface and 100% below chlorophyll maximum; Simeon et al., 2003). CDOM (and DOM) dynamics are not currently included in the model and thus its relative contribution to absorption is determined by the variability of particulate absorption.

3.2.2 Backscattering

Modeled backscattering coefficients by small and large POC (POC1 and POC2, respectively) at 660 nm ($b_{bp1}(660)$ and $b_{bp2}(660)$, respectively) are highest at surface and decrease with depth (Fig. 8). Contribution of POC1 to total particle backscattering is 53–66%. The contribution of picoplankton to backscattering is less dominant than that to absorption, but it is still higher than that of diatoms because of its small size and larger contribution to POC (Stramski and Kiefer, 1991).

3.2.3 Beam attenuation

Beam attenuation, especially by particles (c_p), has been measured often in the equatorial Pacific (e.g. Chung et al., 1996; Bishop, 1999; Gardner et al., 2003). As the contribution of particulate absorption is negligible at 660 nm (Figs. 3b and c), we can assume that c_p is due to scattering by particles. The modeled vertical profile of c_p is similar to the vertical profiles of backscattering coefficients by particles and POC concentration (Figs. 8 and 9b, c), all of which have the maximum at surface and decrease with depth. Both modeled POC and c_p agree with measurements in the equatorial

EGU

Pacific upwelling region (Fig. 9a), which warrants application of the relation between POC and c_p (Eqs. 7 and 8) to this region.

3.3 Optics as a constraint for determining variables and related parameters

3.3.1 Sensitivity to optical parameters

5 The parameter values chosen in this study for the optical model are based on observations (Table 1), but the observed values have substantial variability that arises from environmental and methodological variability. To elucidate how model results are affected by variations in the optical model parameters, we conduct the model sensitivity simulations to them by changing their parameter values individually from 0.7 to 1.3
10 times the standard values, encompassing the bulk of observed values (Table 2).

We find the model results of biogeochemistry, i.e. surface NO_3, $Si(OH)_4$, and maximum chlorophyll and its associated depth, to be most sensitive to changes in the absorption coefficient by CDOM at 440 nm ($a_{CDOM}(440)$). The surface NO_3 increases and $Si(OH)_4$ decreases with the increase of $a_{CDOM}(440)$, due to an increase in contribution
15 by diatoms when $a_{CDOM}(440)$ is higher. The maximum chlorophyll decreases and appears at a deeper layer of 85 m with an $a_{CDOM}(440)$ increase. These model results reveal that the CDOM concentration strongly affects phytoplankton community structure and its dynamics. While CDOM's inherent effects on backscattering and hence beam attenuation coefficient at 660 nm ($C_p(660)$) are negligible, an increase of $a_{CDOM}(440)$
20 yields a $C_p(660)$ decrease due to a decrease in small algal POC. The modeled euphotic layer depth, defined as a depth of 0.1% light level of sea surface, decreases from 120 m to 110 m by varying $a_{CDOM}(440)$ from 0.011 to 0.021 (m^{-1}), primarily as a result of enhanced absorption by CDOM. The change of the euphotic layer depth is relatively small because PAR is more controlled by absorption by water than absorption
25 by underwater particle and CDOM concentration. However, the euphotic layer depth is more sensitive to $a_{CDOM}(440)$ than to the other optical parameters due to significant absorption by CDOM at short wavelengths around 400 nm, at which absorption by water

Bio-optical modeling

M. Fujii et al.

Title Page

Abstract | Introduction

Conclusions | References

Tables | Figures

◄ | ►

◄ | ►

Back | Close

Full Screen / Esc

Printer-friendly Version

Interactive Discussion

EGU

is negligible (Figs. 3a and d).

The observed sensitivity to CDOM concentration is the result of CDOM absorbing light that would otherwise be absorbed by phytoplankton. This effect is more pronounced on picoplankton as they have a relatively higher portion of their energy absorbed in the blue wavelength where CDOM absorbs (they are less packaged and thus have a higher blue to red absorption ratio). Changes in the relative abundance of small and large phytoplankton results in a change in the biogeochemistry of the upper ocean since their metabolic requirements and interaction with other trophic levels are different.

Variation in other optical parameters also contribute to changes in the model results, but their impact is smaller than that of $a_{CDOM}(440)$. The carbon-specific absorption coefficient by NAP at 440 nm ($a_{NAP}^+(440)$) has weaker but similar effects on surface nutrient and maximum chlorophyll concentration as $a_{CDOM}(440)$. The modeled $a_{NAP}/a_p(440)$ is the most sensitive to $a_{NAP}^+(440)$, changing by a factor of 2 from 0.10 to 0.20. The modeled $C_p(660)$ is affected most significantly by the ratio of phytoplankton to particulate organic carbon (R_{POC}^ϕ). The modeled euphotic layer depth does not change from the standard value of 115 m by changing any optical parameters except for $a_{NAP}^+(440)$, which indicates the important role of absorption in the lower layer below chlorophyll maximum in determining the euphotic layer depth. Varying any of the backscattering ratios, regardless of particle type, does not affect the modeled biogeochemistry but does influence $C_p(660)$. However, the sensitivity of $C_p(660)$ to the backscattering ratios depends on particle type, being stronger for NAP and picoplankton and weaker for diatoms and background particles, reflecting the higher backscattering coefficient by picoplankton than by diatoms.

The overall sensitivity study shows that narrowing the observed ranges of optical parameters above is required to reduce uncertainties in reproducing biogeochemistry. In addition, the above analysis suggests that although the dynamics of neither CDOM nor bacteria are currently incorporated explicitly in the model, embedding CDOM as a state variable in the ecosystem model should be given priority over bacteria to improve simulating bio-optical interactions.

3.3.2 Comparison of model results: with and without optics

In ecosystem models that are not coupled to an optical model, values of biogeochemical parameters are tuned to minimize model-data misfits with vertical profiles of nutrient and chlorophyll concentrations and net community production in the euphotic layer (Fig. 5b, c, d). Vertical profile of PAR was not used to calibrate parameters in previous ecosystem models with constant light attenuation coefficients. Modeled zooplankton biomass and NAP concentration cannot be validated because very few corresponding observational data exist.

In order to investigate the value of incorporating a full optical and radiative transfer model into the ecosystem model, we compare two cases, Cases 1 and 2. Case 1 uses only a rudimentary wavelength integrated model for the underwater light field (Eq. 15 below), while Case 2 is the full model using Ecolight to obtain the spectrally resolved underwater light field as described in Sect. 3.

The model structure in Case 1 was modified from Case 2, as follows. PAR is computed from:

$$\text{PAR}(z)(W\ m^{-2}) = \text{PAR}(0) \times \exp\left\{-k_1 z - k_2 \int_{-z}^{0} (\text{Chl1}(z) + \text{Chl2}(z))dz\right\}, \qquad (15)$$

where k_1 is the light attenuation coefficient due to water $(0.046\ (m^{-1}))$ and k_2 is the light attenuation coefficient by chlorophyll $(0.048\ (mgChl\ m^{-3})^{-1}$; e.g. Chai et al., 2002). We carry out two case studies with the non-spectral ecosystem model, Cases 1–1 and 1–2.

In Case 1–1, the light attenuation coefficients are set to the same as in Chai et al. (2002) (Table 1). In this case, as in most previous ecosystem modeling studies, observed PAR values and associated decreases with depth are not referred to in tuning model parameters. Therefore, the parameters are tuned to minimize model-data misfits with vertical profiles of nutrient and chlorophyll concentrations and net community production, which requires modification of the microzooplankton maximum specific

Bio-optical modeling

M. Fujii et al.

EGU

grazing rate ($G1_{max}$) from Case 2 by a factor of 1.2 (Table 1). The model results show similar vertical profiles of Si(OH)$_4$ concentration and net community production, relatively low surface NO$_3$ concentration, and higher and deeper chlorophyll maximum, compared with those in Case 2, although the results of both models are within the observations (Figs. 5b, c, d, e). The modeled PAR in Case 1–1 is higher than in Case 2 by a factor of 1.7 and overestimates the observation (Fig. 5a). The modeled surface NO$_3$ concentration and maximal value of chlorophyll concentration cannot be decreased by changing any parameters other than light attenuation coefficients.

In Case 1–2, vertical profiles of PAR, nutrient and chlorophyll concentrations, and net community production are used for tuning model parameters. The light attenuation coefficients are increased relative to those in Chai et al. (2002), by a factor of 1.2 in k_1 and 1.3 in k_2 (Table 1), to reproduce observed vertical profiles of PAR. Once the light attenuation coefficients are elevated, we can set values of the other parameters to the same as in Case 2 (Table 1) for the best-fit model results. However, without information for NAP concentration, it is difficult to estimate parameter values associated with zooplankton, such as maximum specific grazing rates, because of pronounced nitrogen flow from zooplankton to NAP via fecal pellets. In Case 2 with the bio-optical model, we tune the maximum specific grazing rates so that the model can reproduce the measured contribution of NAP to absorption by total particles by 10–17% (Dupouy et al., 1997 and 2003; Parslow et al., 1998; Bricaud et al., 2002) (Fig. 6b), as described in Sect. 3.2.1.

Phytoplankton community assemblage can also be reproduced by the model with optics (Case 2). In Chai et al. (2002), using the non-spectrally-resolved ecosystem model, they tuned the water-column phytoplankton assemblage so that the percentage of diatoms to the total phytoplankton biomass is nearly 16%, referring to the observed ranges from 5% to 20% (Bidigare and Ondrusek, 1996). With the spectrally-resolved bio-optical model (Case 2), we could tune vertical phytoplankton assemblage more accurately, referring to not only measurements of each phytoplankton biomass but also those of contribution of diatoms to total phytoplankton derived from optical properties

EGU

(absorption and backscattering).

These results suggest that both ecosystem model results with or without optics can reproduce the observed fundamental biogeochemical properties in the equatorial Pacific, as long as the correct diffuse light attenuation is used. Since the PAR data are not consistent with the simple chlorophyll formulation used previously in Chai et al. (2002), another source of diffuse light attenuation is needed for the model that can take into account contribution by NAP and CDOM. Our bio-optical model provides such a value.

In addition, the coupled model results illustrate its capability to be constrained using observations of optical variables and thus its ability in improving model performance, which currently cannot be done with available biological properties alone. Additional constituents, which should be added to future ecosystem models, such as DOM, bacteria, and coccoliths (e.g. Fujii and Chai, 2007), are likely to improve the optics-simulation model fit assuming relevant data on their abundance can be obtained.

While we were able to reproduce most of the observations by simply changing the diffuse attenuation values in the model lacking optics (Case 1–2), this approach is not likely to work in temporally varying simulations where the diffuse attenuation coefficient changes in time; any changes in the relative proportion of the biogeochemical variables contributing to absorption (and to a lesser degree to backscattering) would result in changes in the diffuse attenuation parameters in Eq. (15). Simulating these changes requires having the appropriate biogeochemical constituents and related optical properties, most of which are captured by the bio-optical model (with the important exception of CDOM).

4   Summary and remarks

We developed an ecosystem model that explicitly represents biogeochemically and optically two phytoplankton and two zooplankton functional groups, as well as multiple nutrients and non-algal particles (NAP). We applied the model to the equatorial Pacific upwelling region and found that utilizing an optical model to convert from ecosystem

EGU

model state variables to optical parameters and a realistic subsurface light provides: (1) more data to compare model output with providing a more rigorous test on model formulation and choice of parameter values, especially for those that are difficult to measure in high resolution in time and space, (2) the required input to obtain a realistic subsurface light field by linking the optics to a radiative-transfer model (Ecolight), and (3) improved simulation realism with respect to key biogeochemical processes, such as photosynthesis, which are crucial for assessing oceanic carbon cycling and food web dynamics. The additional optical measurements, being routinely available from research vessels, autonomous platforms, and space-borne observations, can now be used directly for comparison and testing of the output of our new coupled bio-optical model. This is an improvement over the limited number of variables that can be used to test our previous ecosystem models with no explicit optical properties.

Model sensitivity studies on optical parameters suggest that CDOM may have an important role in phytoplankton dynamics, nutrient cycling, and light field in the euphotic layer. Incorporating radiative transfer models to ecosystem models would also contribute to improving the realistic simulations of physical-bio-optical interactions such as chlorophyll modulation of water temperature (e.g. Nakamoto et al., 2000), although these capabilities were not tested here. In the future, real time optical data should be obtained and used in an assimilation mode, increasing the realism of ecosystem simulations such as prediction of the harmful algal bloom dynamics in coastal regions, a prediction that is extremely useful for monitoring near shore water quality and its impact on marine living resources and aquaculture.

Appendix A

Physical-ecosystem model

A1   Governing equations

The model equations describing each compartment all take the form:

$$\frac{\partial C_i(z)}{\partial t}[\text{mmol m}^{-3}\text{day}^{-1}] \text{ or } [\text{mg m}^{-3}\text{day}^{-1}] = \text{PHYSICS}(C_i(z)) + \text{BIOLOGY}(C_i(z)), \quad \text{(A1)}$$

$i = 1, \ldots, 13$.

The model state variables (C_i) are picoplankton (P1 (mmolN m^{-3}), C1 (mmolC m^{-3}), and Chl1 (mgChl m^{-3})), diatoms (P2 (mmolN m^{-3}), C2 (mmolC m^{-3}), and Chl2 (mgChl m^{-3})), microzooplankton (Z1 (mmolN m^{-3})), mesozooplankton (Z2 (mmolN m^{-3})), nitrate (NO_3 (mmolN m^{-3})), ammonium (NH_4 (mmolN m^{-3})), silicate ($Si(OH)_4$ (mmolSi m^{-3})), non-algal particles (NAP (mmolN m^{-3})), and biogenic silica ($bSiO_2$ (mmolSi m^{-3})).

The term PHYSICS($C_i(z)$) represents the contribution to the concentration change due to physical processes, including vertical advection and eddy diffusion:

$$\text{PHYSICS}(C_i(z))[\text{mmol m}^{-3}\text{day}^{-1}] \text{ or } [\text{mg m}^{-3}\text{day}^{-1}] = \underbrace{-W\frac{\partial C_i(z)}{\partial z}}_{\text{advection}} + \underbrace{\frac{\partial}{\partial z}(A_{Tv}\frac{\partial C_i(z)}{\partial z})}_{\text{eddy diffusivity}}, \quad \text{(A2)}$$

where W is vertical velocity, and A_{Tv} is vertical coefficient. The values are the same as Chai et al. (2002). The term BIOLOGY (Ci(z)) represents biological sources and sinks of that compartment. In the euphotic zone (the upper 120 m), the biological terms, BIOLOGY(Ci(z)) are:

$$\text{BIOLOGY}(P1(z))[\text{mmol N m}^{-3}\text{day}^{-1}] = \underbrace{NP1(z)+RP1(z)}_{\text{growth}} - \underbrace{G_1(z)}_{\text{grazing by Z1}}, \quad \text{(A3)}$$

EGU

$$\text{BIOLOGY}(C1(z))[\text{mmol Cm}^{-3}\text{day}^{-1}]= \underbrace{P^{C1}(z)-\xi_{P1}(z)\,(NP1(z)+RP1(z))}_{\text{growth}}-\underbrace{G_1(z)\times\frac{C1(z)}{P1(z)}}_{\text{grazing by Z1}}, \tag{A4}$$

$$\text{BIOLOGY}(Chl1(z))[\text{mgChlm}^{-3}\text{day}^{-1}]= \underbrace{\rho_{\text{Chl1}}(z)(NR1(z)+RP1(z))}_{\text{growth}}-\underbrace{G_1(z)\times\frac{\text{Chl1}(z)}{P1(z)}}_{\text{grazing by Z1}}, \tag{A5}$$

$$\text{BIOLOGY}(P2(z))[\text{mmol Nm}^{-3}\text{day}^{-1}]= \underbrace{NP2(z)+RP2(z)}_{\text{Growth}}-\underbrace{G_2(z)}_{\text{grazing by Z2}}-\underbrace{\gamma_3 P2(z)}_{\text{mortality}}-\underbrace{\frac{\partial}{\partial z}(W_1 P2(z))}_{\text{sinking}}, \tag{A6}$$

$$\text{BIOLOGY}(C2(z))[\text{mmol Cm}^{-3}\text{day}^{-1}]= \underbrace{P^{C2}(z)-\xi_{P2}(z)\,(NP2(z)+RP2(z))}_{\text{growth}}-\underbrace{G_2(z)\times\frac{C2(z)}{P2(z)}}_{\text{grazing by Z2}}-\underbrace{\frac{\partial}{\partial z}(W_1 C2(z))}_{\text{sinking}}-\underbrace{\gamma_3 C2(z)}_{\text{mortality}}, \tag{A7}$$

$$\text{BIOLOGY}(Chl2(z))[\text{mgChlm}^{-3}\text{day}^{-1}]= \underbrace{\rho_{\text{Chl2}}(z)(NR2(z)+RP2(z))}_{\text{growth}}-\underbrace{G_2(z)\times\frac{\text{Chl2}(z)}{P2(z)}}_{\text{grazing by Z1}}$$

5

$$-\underbrace{\frac{\partial}{\partial z}(W_1\text{Chl2}(z))}_{\text{sinking}}-\underbrace{\gamma_3\text{Chl2}(z)}_{\text{mortality}}, \tag{A8}$$

$$\text{BIOLOGY}(Z1(z))[\text{mmolNm}^{-3}\text{day}^{-1}]= \underbrace{\gamma G_1(z)}_{\text{grazing on P1}}-\underbrace{G_3(z)}_{\text{predation by Z2}}-\underbrace{\text{reg}_1 Z1(z)}_{\text{excretion}}, \tag{A9}$$

$$\text{BIOLOGY}(Z2(z))[\text{mmolNm}^{-3}\text{day}^{-1}]= \underbrace{\gamma_1(G_2(z)+G_3(z)+G_4(z))}_{\text{fecal pullet}}-\underbrace{\text{reg}_2 Z2(z)}_{\text{excretion}}-\underbrace{\gamma_2 Z2(z)^2}_{\text{loss}}, \tag{A10}$$

$$\text{BIOLOGY}(NO_3(z))[\text{mmolNm}^{-3}\text{day}^{-1}]=-\underbrace{NP1(z)}_{\text{uptake by P1}}-\underbrace{NP2(z)}_{\text{uptake by P2}}+\underbrace{\gamma_5 NH_4(z)}_{\text{nitrification}}, \tag{A11}$$

$$\text{BIOLOGY}(NH_4(z))[\text{mmolNm}^{-3}\text{day}^{-1}]=-\underbrace{RP1(z)}_{\text{uptake by P1}}-\underbrace{RP2(z)}_{\text{uptake by P2}}$$
$$+\underbrace{\text{reg}_1 Z1(z)+\text{reg}_2 Z2(z)}_{\text{excretion}}+\underbrace{\gamma_7 \text{NAP}(z)}_{\text{PON remineralization}}-\underbrace{\gamma_5 NH_4(z)}_{\text{nitrification}}, \tag{A12}$$

Bio-optical modeling

M. Fujii et al.

Title Page

Abstract	Introduction
Conclusions	References
Tables	Figures

|◄ | ►|
◄ | ►
Back | Close

Full Screen / Esc

Printer-friendly Version

Interactive Discussion

EGU

$$\text{BIOLOGY}(\text{Si}(\text{OH})_4(z))[\text{mmolSim}^{-3}\text{day}^{-1}] = -\underbrace{R_{\text{SiN}}(NP2(z)+RP2(z))}_{\text{silicification}} + \underbrace{\gamma_4 b\text{SiO}_2(z)}_{\text{bSiO2 dissolution}}, \quad \text{(A13)}$$

$$\text{BIOLOGY}(\text{NAP}(z))[\text{mmolNm}^{-3}\text{day}^{-1}] = \underbrace{(1-\gamma_0)G_1(z)+(1-\gamma_1)(G_2(z)+G_3(z)+G_4(z))}_{\text{fecal pullet}} - \underbrace{G_4(z)}_{\text{grazing by Z2}} + \underbrace{\gamma_3 P2(z)}_{\text{P2 mortality}}$$
$$- \underbrace{\gamma_7 \text{NAP}(z)}_{\text{PON remineralization}} - \underbrace{\frac{\partial}{\partial z}(W_2 \text{NAP}(z))}_{\text{sinking}}, \quad \text{(A14)}$$

$$\text{BIOLOGY}(b\text{SiO}_2(z))[\text{mmolSim}^{-3}\text{day}^{-1}] = \underbrace{R_{\text{SiN}}G_2(z)}_{\text{fecal pullet}} - \underbrace{\gamma_4 b\text{SiO}_2(z)}_{\text{dissolution}} + \underbrace{\gamma_3 R_{\text{SiN}}P2(z)}_{\text{P2 mortality}} - \underbrace{\frac{\partial}{\partial z}(W_4 b\text{SiO}_2(z))}_{\text{sinking}}. \quad \text{(A15)}$$

Each biological process is described in the next subsection. See Table 1 for abbreviations.

A2 Formulation of biological processes

(NO$_3$ uptake by picoplankton)

$$NP1(z)[\text{mmolSim}^{-3}\text{day}^{-1}] = V_N^C\text{ref}_{P1} \times \frac{1-\text{fnit}_{P1}(z)}{1.015-\text{fnit}_{P1}(z)} \times \text{Tfunc}(z) \times \underbrace{\frac{NO_3(z)}{K_{NO_3}+NO_3(z)}}_{NO_3\,\text{regulation}} \times \underbrace{e^{-\Psi NH_4(z)}}_{NH_4\,\text{inhibition}} \times C1(z). \quad \text{(A16)}$$

where

$$V_N^C\text{ref}_{P1}[\text{mmolN mmolC}^{-1}\,\text{day}^{-1}] = P_{\text{ref}}^{C1} \times Q\max, \quad \text{(A17)}$$

$$\text{fnit}_{P1}(z) = \frac{uQ1(z)-Q\min}{Q\max-Q\min}, \quad \text{(A18)}$$

$$uQ1(z)[\text{mmolN mmolC}^{-1}] = \frac{P1(z)}{Cl(z)}, \quad Q\min < uQ1(z) < Q\max, \quad \text{(A19)}$$

$$\text{Tfunc}(z) = \exp\left\{-\frac{Ea}{R} \times \left(\frac{1}{\text{Temp}(z)+273.15} - \frac{1}{T_{\text{ref}}}\right)\right\}. \quad \text{(A20)}$$

EGU

(NH$_4$ uptake by picoplankton)

$$RP1(z)[\text{mmolC m}^{-3}\text{ day}^{-1}]=V_N^C\text{ref}_{P1}\times\frac{1-\text{fnit}_{P1}(z)}{1.015-\text{fnit}_{P1}(z)}\times\text{Tfunc}(z)\times\underbrace{\frac{\text{NH}_4(z)}{K_{\text{NH}_4}+\text{NH}_4(z)}}_{\text{NH}_4\text{ regulation}}\times C1(z). \tag{A21}$$

(Carbon uptake by picoplankton)

$$P^{C1}(z)[\text{mmolC m}^{-3}\text{ day}^{-1}]=P_{\text{ref}}^{C1}\times\text{fnit}_{P1}(z)\times\text{Tfunc}(z)\times\left\{1-\exp(\frac{-\alpha\times\theta^{C1}(z)\times\text{PAR}(z)}{P_{\text{ref}}^{C1}\times\text{fnit}_{P1}(z)\times\text{Tfunc}(z)})\right\}\times C1(z), \tag{A22}$$

where

$$\theta^{C1}(z)[\text{mgChl mmolC}^{-1}]=\frac{\text{Chl1}(z)}{C1(z)}, \tag{A23}$$

$$\xi_{P1}(z)[\text{mmolC mmolN}^{-1}]=\xi_{\text{NO3}}\times\max\left(\frac{NP1(z)}{NP1(z)+RP1(z)},0.5\right). \tag{A24}$$

(Chlorophyll uptake by picoplankton)

$$\rho_{\text{Chl1}}(z)[\text{mgChl mmolN}^{-1}]=\frac{\theta_{\max}^N\times P_{\text{ref}}^{C1}\times\text{fnit}_{P1}(z)\times\text{Tfunc}(z)\times\left\{1-\exp\left(\frac{-\alpha\times\theta^{C1}(z)\times\text{PAR}(z)}{P_{\text{ref}}^{C1}\times\text{fnit}_{P1}(z)\times\text{Tfunc}(z)}\right)\right\}}{\alpha\times\theta^{C1}(z)\times\text{PAR}(z)}. \tag{A25}$$

(NO$_3$ and NH$_4$ uptake by diatoms)

$$If \frac{1}{R_{\text{SiN}}}\frac{\text{Si(OH)}_4(z)}{K_{\text{Si(OH)}_4}+\text{Si(OH)}_4(z)} > \frac{\text{NH}_4(z)}{K_{P2\_\text{NH}_4}+\text{NH}_4(z)}, \tag{A26}$$

$$NP2(z)[\text{mmolNm}^{-3}\text{day}^{-1}]=V_N^C\text{ref}_{P2}\times\left(\frac{1}{R_{\text{SiN}}}\underbrace{\frac{\text{Si(OH)}_4(z)}{K_{\text{Si(OH)}_4}+\text{Si(OH)}_4(z)}}_{\text{Si(OH)}_4\text{ regulation}}-\underbrace{\frac{NH_4(z)}{K_{\text{S2}-\text{NH}_4}+\text{NH}_4(z)}}_{\text{NH}_4\text{ regulation}}\right) \\ \times\frac{1-\text{fnit}_{P2}(z)}{1.015-\text{fnit}_{P2}(z)}\times\text{Tfunc}(z)\times C2(z), \tag{A27}$$

$$RP2(z)[\text{mmolNm}^{-3}\text{day}^{-1}]=V_N^C\text{ref}_{P2}\times\frac{1-\text{fnit}_{P2}(z)}{1.015-\text{fnit}_{P2}(z)}\times\text{Tfunc(z)}\times\underbrace{\frac{\text{NH}_4(z)}{K_{\text{S2}-\text{NH}_4}+\text{NH}_4(z)}}_{\text{NH}_4\text{ regulation}}\times C2(z).$$

(A28)

where

$$V_N^C\text{ref}_{P2}[\text{mmolN mmolC}^{-1}\text{ day}^{-1}]=P_{\text{ref}}^{C2}\times Q\,\text{max},$$

(A29)

$$\text{fnit}_{P2}(z)=\frac{uQ2(z)-Q\,\text{min}}{Q\,\text{max}-Q\,\text{min}},$$

(A30)

$$uQ2(z)[\text{mmolN mmolC}^{-1}]=\frac{P2(z)}{C2(z)},Q\,\text{min}<uQ2(z)<Q\,\text{max}$$

(A31)

$$\text{If }\frac{1}{R_{\text{SiN}}}\frac{\text{Si(OH)}_4(z)}{K_{\text{Si(OH)}_4}+\text{Si(OH)}_4(z)}\le\frac{\text{NH}_4(z)}{K_{P2\_\text{NH}_4}+\text{NH}_4(z)},$$

(A32)

$$NP2(z)=0,$$

(A33)

$$RP2(z)[\text{mmolNm}^{-3}\text{day}^{-1}]=V_N^C\text{ref}_{P2}\times\frac{1}{R_{\text{SiN}}}\frac{\text{Si(OH)}_4(z)}{K_{\text{Si(OH)}_4}+\text{Si(OH)}_4(z)}$$
$$\times\frac{1-\text{fnit}_{P2}(z)}{1.015-\text{fnit}_{P2}(z)}\times\text{Tfunc(z)}\times C2(z).$$

(A34)

(Carbon uptake by P2)

$$P^{C2}(z)[\text{mmolC m}^{-3}\text{ day}^{-1}]=P_{\text{ref}}^{C2}\times\text{fnit}_{P2}(z)\times\text{Tfunc}(z)\times\left\{1-\exp\left(\frac{-\alpha\times\theta^{C2}(z)\times\text{PAR}(z)}{P_{\text{ref}}^{C2}\times\text{fnit}_{P2}(z)\times\text{Tfunc}(z)}\right)\right\}\times C2(z),$$

(A35)

where

$$\theta^{C2}(z)[\text{mgChl mmolC}^{-1}]=\frac{Chl2(z)}{C2(z)},$$

(A36)

Bio-optical modeling

M. Fujii et al.

EGU

$$\xi_{P2}(z)[\text{mmolC mmolN}^{-1}] = \xi_{NO3} \times \max\left(\frac{NP2(z)}{NP2(z) + RP2(z)}, 0.5\right). \quad (A37)$$

(Chlorophyll uptake by P2)

$$\rho_{\text{Chl2}}(z)[\text{mgChl mmolN}^{-1}] = \frac{\theta_{\text{max}}^{N} \times P_{\text{ref}}^{C2} \times \text{fnit}_{P2}(z) \times \text{Tfunc}(z) \times \left\{1 - \exp\left(\frac{-\alpha \times \theta^{C2}(z) \times \text{PAR}(z)}{P_{\text{ref}}^{C2} \times \text{fnit}_{P2}(z) \times \text{Tfunc}(z)}\right)\right\}}{\alpha \times \theta^{C2}(z) \times \text{PAR}(z)}. \quad (A38)$$

(Grazing on picoplankton by microzooplankton)

$$G_1(z)[\text{mmolN m}^{-3}\text{day}^{-1}] = G1_{\text{max}} \underbrace{\frac{P1(z)}{K1_{gr} + P1(z)}}_{\text{food limitation}} \underbrace{\frac{P1(z)}{P1_{\text{ave}}}}_{\text{depth modification}} Z1(z), \quad (A39)$$

$$P1_{\text{ave}}[\text{mmolN m}^{-3}\text{day}^{-1}] = \frac{1}{Z'} \int_{-Z'}^{0} P1(z)\, dz, \quad (A40)$$

where Z' is the depth of the euphotic zone (120 m).
(Grazing or predation on diatoms, microzooplankton, and NAP by mesozooplankton)

$$G_2(z)[\text{mmolNm}^{-3}\text{day}^{-1}] = G2_{\text{max}} \frac{\zeta_1 P2(z)}{K2_{gr} + \zeta_1 P2(z) + \zeta_2 Z1(z) + \zeta_3 \text{NAP}(z)} Z2(z), \quad (A41)$$

$$G_3(z)[\text{mmolNm}^{-3}\text{day}^{-1}] = G2_{\text{max}} \frac{\zeta_2 Z1(z)}{K2_{gr} + \zeta_1 P2(z) + \zeta_2 Z1(z) + \zeta_3 \text{NAP}(z)} Z2(z), \quad (A42)$$

$$G_4(z)[\text{mmolNm}^{-3}\text{day}^{-1}] = G2_{\text{max}} \frac{\zeta_3 \text{NAP}(z)}{K2_{gr} + \zeta_1 P2(z) + \zeta_2 Z1(z) + \zeta_3 \text{NAP}(z)} Z2(z), \quad (A43)$$

where

$$\zeta_1 = \frac{\rho_1 P2(z)}{\rho_1 P2(z) + \rho_2 Z1(z) + \rho_3 \text{NAP}(z)}, \quad (A44)$$

Bio-optical modeling

M. Fujii et al.

◄◄ | ►►

◄ | ►

Back | Close

Full Screen / Esc

Printer-friendly Version

Interactive Discussion

EGU

$$\zeta_2 = \frac{\rho_2 Z1(z)}{\rho_1 P2(z) + \rho_2 Z1(z) + \rho_3 \mathrm{NAP}(z)}, \tag{A45}$$

$$\zeta_3 = \frac{\rho_3 \mathrm{NAP}(z)}{\rho_1 P2(z) + \rho_2 Z1(z) + \rho_3 \mathrm{NAP}(z)}. \tag{A46}$$

Appendix B

Chlorophyll-specific absorption coefficients by phytoplankton in high and low light environments

We need highest and lowest chlorophyll-specific absorption coefficients by picoplankton ($a^*_{\phi1(\text{high light})}(\lambda)$ and $a^*_{\phi1(\text{low light})}(\lambda)$) and diatoms ($a^*_{\phi2(\text{high light})}(\lambda)$ and $a^*_{\phi2(\text{low light})}(\lambda)$) to obtain chlorophyll-specific absorption coefficients at each wavelength and depth from Eqs. (1) and (2) in Sect. 2.2. Although many previous studies have measured the chlorophyll-specific absorption coefficients by various phytoplankton species, the values are highly variable, especially for picoplankton in the surface water at around 440 nm (e.g. Moore et al., 1995; Allali et al., 1997; Culver and Perry, 1999; Ciotti et al., 2002; Devred et al., 2006). This implies complicated small phytoplankton assemblage with different pigment packaging in reality while the small phytoplankton (P1) is represented by one species (picoplankton) in the model. In addition, the measured specific absorption coefficient by small phytoplankton is often obtained by dividing the absorption coefficient by not only chlorophyll but also other pigments such as pheophytin (pheopigments).

The highest chlorophyll-specific absorption coefficient by diatoms at 440 nm ($a^*_{\phi2(\text{high light})}(440)$) is set to 0.012 ($\mathrm{m^2 mg^{-1}}$), based on an observed mean value of microplankton in the surface water (Fig. 7 in Ciotti et al., 2002). We assume that a ratio of highest to lowest chlorophyll-specific absorption coefficient at 440 nm in the equatorial Pacific is around 1.5 for each phytoplankton, attributing to observed chlorophyll-

EGU

specific absorption coefficients by total phytoplankton at 440 nm in each depth, which varies from 0.07 (m^2 mg^{-1}) in the surface water ($a^*_{\phi(\text{high light})}$ (440)) to 0.045 (m^{2}mg^{-1}) at the bottom of the euphotic layer ($a^*_{\phi(\text{low light})}$ (440)) (Fig. 5 in Allali et al., 1997). Therefore, $a^*_{\phi2(\text{low light})}$ (440) is estimated to be about 0.008 (m^2 mg^{-1}). We also assume that a ratio of picoplankton to total phytoplankton chlorophyll and that of diatoms to total phytoplankton chlorophyll are around 0.83 and 0.17, respectively, and are uniform with depth (e.g. Chavez, 1989; Peña et al., 1990; Bidigare and Ondrusek, 1996). Based on Ciotti et al. (2002), Devred et al. (2006) reconstructed the specific absorption spectra of phytoplankton communities as a linear combination of absorption spectra of small and large cells:

$$a^*_\phi(\lambda, z)[\text{m}^2\ \text{mg}^{-1}]=Fa^*_{\phi1}(\lambda, z)=(1-F)a^*_{\phi2}(\lambda, z), \tag{B1}$$

where F is the phytoplankton size fraction.

With the assumption above, we estimate highest and lowest chlorophyll-specific absorption coefficients by picoplankton at 440 nm ($a^*_{\phi1(\text{high light})}$ (440) and $a^*_{\phi1(\text{low light})}$ (440), respectively) as follows:

$$a^*_{\phi1(\text{high light})}(440)[\text{m}^2\text{mg}^{-1}]=\frac{\left\{a^*_{\phi(\text{high light})}(440)-0.17\times a^*_{\phi2(\text{high light})}(440)\right\}}{0.83}, \tag{B2}$$

$$a^*_{\phi1(\text{low light})}(440)[\text{m}^2\text{mg}^{-1}]=\frac{\left\{a^*_{\phi(\text{low light})}(440)-0.17\times a^*_{\phi2(\text{low light})}(440)\right\}}{0.83}. \tag{B3}$$

From these equations, we derive $a^*_{\phi1(\text{high light})}$ (440) of 0.082 (m^2 mg^{-1}) and $a^*_{\phi1(\text{low light})}$ (440)) of 0.053 (m^2 mg^{-1}), which agree well with the observed chlorophyll-specific absorption coefficients by picoplankton (e.g. Ciotti et al., 2002). The highest and lowest chlorophyll-specific absorption coefficients by picoplankton and diatoms at other wavelengths are derived by fitting spectral profiles of Ciotti and Bricaud (2006) and Ciotti et al. (2002), respectively, to coincide at 440 nm.

Bio-optical modeling

M. Fujii et al.

Title Page

Abstract	Introduction
Conclusions	References
Tables	Figures

|◄ | ►|
◄ | ►

Back | Close

Full Screen / Esc

Printer-friendly Version

Interactive Discussion

EGU

References

Allali, K., Bricaud, A., and Claustre, H.: Spatial variations in the chlorophyll-specific absorption coefficients of phytoplankton and photosynthetically active pigments in the equatorial Pacific, J. Geophys. Res., 102(C6), 12 413–12 423, 1997.

Babin, M., Morel, A., Fournier-Sicre, V., Fell, F., and Stramski, D.: Light scattering properties of marine particles in coastal and open ocean waters as related to the particle mass concentration, Limnol. Oceanogr., 48(2), 843–859, 2003a.

Babin, M., Stramski, D., Ferrari, G. M., Claustre, H., Bricaud, A., Obolensky, G., and Hoepffner, N.: Variations in the light absorption coefficients of phytoplankton, nonalgal particles, and dissolved organic matter in coastal waters around Europe, J. Geophys. Res. 108(C7), 3211, doi:10.1029/2001JC000882, 2003b.

Barber, R. T., Sanderson, M. P., Lindley, S. T., Chai, F., Newton, J., Trees, C. C., Foley, D. G., and Chavez, F. P.: Primary productivity and its regulation in the equatorial Pacific during and following the 1991–1992 El Niño, Deep-Sea Res. Part II, 43(4–6), 933–969, 1996.

Behrenfeld, M. J. and Boss, E.: Beam attenuation and chlorophyll concentration as alternative optical indices of phytoplankton biomass, J. Mar. Res., 64, 431–451, 2006.

Behrenfeld, M. J., Boss, E., Siegel, D. A., and Shea, D. M.: Carbon-based ocean productivity and phytoplankton physiology from space, Global Biogeochem. Cycles, 19, GB1006, doi:10.1029/2004GB002299, 2005.

Behrenfeld, M. J. and Falkowski, P. G.: Photosynthetic rates derived from satellite-based chlorophyll concentration, Limnol. Oceanogr., 42, 1–20, 1997.

Bidigare, R. R. and Ondrusek, M. E.: Spatial and temporal variability of phytoplankton pigment distributions in the central equatorial Pacific Ocean, Deep-Sea Res. Part II, 43(4–6), 809–833, 1996.

Bishop, J. K. B.: Transmissometer measurement of POC, Deep-Sea Res. Part I, 46, 355–369, 1999.

Bio-optical modeling

M. Fujii et al.

|◄ | ►|

◄ | ►

Back | Close

Full Screen / Esc

Printer-friendly Version

Interactive Discussion

EGU

Bissett, W. P., Carder, K. L., Walsh, J. J., and Dieterle, D. A.: Carbon cycling in the upper waters of the Sargasso Sea: II. Numerical simulation of apparent and inherent optical properties, Deep-Sea Res. Part I, 46, 271–317, 1999.

Boss, E. and Pegau, W. S.: The relationship of light scattering at an angle in the backward direction ot the backscattering coefficient, Appl. Opt., 40, 5503–5507, 2001.

Boss, E., Pegau, W. S., Lee, M., Twardowski, M. S., Shybanov, E., Korotaev, G., and Baratange, F.: The particulate backscattering ratio at LEO 15 and its use to study particles composition and distribution, J. Geophys. Res., 109(C1), C01014, doi:10.1029/2002JC001514, 2004.

Bricaud, A., Roesler, C. S., Parslow, J. S., and Ishizaka, J.: Bio-optical studies during the JGOFS-equatorial Pacific program: a contribution to the knowledge of the equatorial system, Deep-Sea Res. Part II, 49, 2583–2599, 2002.

Chai, F., Dugdale, R. C., Peng, T.-H., Wilkerson, F. P., and Barber, R. T.: One-dimensional ecosystem model of the equatorial Pacific upwelling system. Part I: model development and silicon and nitrogen cycle, Deep-Sea Res. Part II, 49, 2713–2745., 2002.

Chai, F., Barber, R. T., and Lindley, S. T.: Origin and maintenance of high nutrient condition in the equatorial Pacific, Deep-Sea Res. Part II, 42(4–6), 1031–1064, 1996.

Chavez, F. P.: Size distribution of phytoplankton in the central and eastern tropical Pacific, Global Biogeochem. Cycles, 3, 27–35, 1989.

Chavez, F. P., Buck, K. R., Coale, K. H., Martin, J. H., DiTullio, G. R., Welshmeyer, N. A., Jacobson, A. C., and Barber, R. T.: Growth rates, grazing, sinking and iron limitation of equatorial Pacific phytoplankton, Limnol. Oceanogr., 36, 1816–1833, 1991.

Cho, B. C. and Azam, F.: Biogeochemical significance of bacterial biomass in the ocean's euphotic zone, Mar. Ecol. Prog. Ser., 63, 253–259, 1990.

Chung, S. P., Gardner, W. D., Richardson, M. J., Walsh, I. D., and Landry, M. R.: Beam attenuation and microorganisms: Spatial and temporal variations in small particles along 140° W during 1992 JGOFS-EqPac transects, Deep-Sea Res. Part II, 43, 1205–1226, 1996.

Ciotti, A. M. and Bricaud, A.: Retrievals of a size parameter for phytoplankton and spectral light absorption by colored detrital matter from water-leaving radiances at SeaWiFS channels in a continental shelf region off Brazil, Limnol. Oceanogr., Methods, 4, 237–253, 2006.

Ciotti, A. M., Lewis, M. R., and Cullen, J. J.: Assessment of the relationship between dominant cell size in natural phytoplankton communities and the spectral shape of the absorption coefficient, Limnol. Oceanogr., 47(2), 404–417, 2002

Cloern, J. E., Grenz, C., and Vidergar-Lucas, L.: An empirical model of the phytoplankton

Title Page

Abstract | Introduction

Conclusions | References

Tables | Figures

|◄ | ►|

◄ | ►

Back | Close

Full Screen / Esc

Printer-friendly Version

Interactive Discussion

EGU

chlorophyll:carbon ratio – the conversion factor between productivity and growth rate, Limnol. Oceanogr., 40(7), 1313–1321, 1995.

Culver, M. E. and Perry, M. J.: The response of photosynthetic absorption coefficients to irradiance in culture and in tidally mixed estuarine waters, Limnol. Oceanogr., 44(1), 24–36, 1999.

Denman, K. L.: Modelling planktonic ecosystems: parameterizing complexity, Prog. Oceanogr., 57, 429–452, 2003.

Denman K. L. and Peña, M. A.: The response of two coupled one-dimensional mixed layer/planktonic ecosystem models to climate change in the NE subarctic Pacific Ocean, Deep Sea Res. II, 49, 5739–5757, 2002.

Devred, E., Sathyendranath, S., Stuart, V., Maass, H., Ulloa, O., and Platt, T.: A two-component model of phytoplankton absorption in the open ocean: Theory and applications, J. Geophys. Res., 111, C03011, doi:10.1029/2005JC002880, 2006.

Dickey, T. D., Lewis, M. R., and Chang, G. C.: Optical oceanography: recent advances and future directions using global remote sensing and in situ observations, Rev. Geophys., 44(1), RG 1001, doi:10.1029/2003RG000148, 2006.

Dupouy, C., Loisel, H., Neveux, J., Brown, S. L., Moulin, C., Blanchot, J., Le Bouteiller, A., and Landry, M. R.: Microbial absorption and backscattering coefficients from in situ and POLDER satellite data during an El Niño-Southern Oscillation cold phase in the equatorial Pacific (180°), J. Geophys. Res., 108(C12), 8138, doi:10.1029/2001JC001298, 2003.

Dupouy, C., Neveux, J., and André, J. M.: Spectral absorption coefficient of photosynthetically active pigments in the equatorial Pacific Ocean (165° E–150° W), Deep-Sea Res. Part II, 44(9–10), 1881–1906, 1997.

DuRand, M. D., Olson, R. J., and Chisholm, S. W.: Phytoplankton population dynamics at the Bermuda Atlantic Time-series station in the Sargasso Sea, Deep-Sea Res. Part II, 48, 1983–2003, 2001.

Duysens, L. M. N.: The flattering effect of the absorption spectra of suspensions as compared to that of solutions, Biochem. Biophys. Acta, 19, 1–12, 1956.

Eppley, R. W., Chavez, F. P., and Barber, R. T.: Standing stocks of particulate carbon and nitrogen in the Equatorial Pacific at 150° W, J. Geophys. Res., 97, 655–661, 1992.

Falkowski, P. G., Dubinsky, Z., and Wyman, K.: Growth-irradiance relationships in phytoplankton, Limnol. Oceanogr., 30, 311–321, 1985.

Fournier, G. and Forand, J. L.: Analytic phase function for ocean water, in: Ocaen Optics XII,

Bio-optical modeling

M. Fujii et al.

Title Page

Abstract	Introduction
Conclusions	References
Tables	Figures

◀◀ ▶▶

◀ ▶

Back Close

Full Screen / Esc

Printer-friendly Version

Interactive Discussion

EGU

edited by: Jaffe, J. S., Proc. SPIE, 2258, 194–201, 1994.

Friedrichs, M. A. M., Dusenberry, J. A., Anderson, L. A., Armstrong, R., Chai, F., Christian, J. R., Doney, S. C., Dunne, J., Fujii, M., Hood, R., McGillicuddy, D., Moore, J. K., Schartau, M., Spitz, Y. H., and Wiggert, J. D.: Assessment of skill and portability in regional marine biogeochemical models: the role of multiple planktonic groups, J. Geophys. Res., doi:10.1029/2006JC003852, 2007.

Fujii, M. and Chai, F.: Modeling carbon and silicon cycling in the equatorial Pacific, Deep-Sea Res. Part II, doi:10.1016/j.dsr2.2006.12.005, 2007.

Gardner, W. D., Richardson, M. J., Carlson, C. A., Hansell, D., and Mishonov, A. V.: Determining true particulate organic carbon: bottles, pumps and methodologies, Deep-Sea Res. Part II, 50, 655–674, 2003.

Geidar, R. J.: Light and temperature dependence of the carbon to chlorophyll a ratio in microalgae and cynobacteria: implications for physiology and growth of phytoplankton, New Phytol., 106, 1–34, 1987.

Geidar, R. J., MacIntyre, H. L., and Kana, T. M.: A dynamic regulatory model of phytoplanktonic acclimation to light, nutrients, and temperature, Limnol. Oceanogr., 43, 679–694, 1998.

Gregg, W. W. and Carder, K. L.: A simple spectral solar irradiance model for cloudless marine atmospheres, Limnol. Oceanogr., 35, 1657–1675, 1990.

Gregg, W. W., Ginoux, P., Schopf, P. S., and Casey, N. W.: Phytoplankton and iron: validation of a global three-dimensional ocean biogeochemical model, Deep-Sea Res. Part II, 50, 3143–3169, 2003.

Gunderson, K., Orcutt, K. M., Purdie, D. A., Michaels, A. F., and Knap, A. H.: Particulate organic carbon mass distribution at the Bermuda Atlantic time-series Study (BATS) site, Deep-Sea Res. Part II, 48, 1697–1718, 2001.

IOCCG: Remote sensing of inherent optical properties: Fundamentals, test of algorithms, and applications, edited by: Lee, Z.-P., Reports of the international ocean-colour coordinating group, No.5, IOCCG, Dartmouth, Canada, 2006.

Iturriaga, R. and Siegel, D. A.: Microphotometric characterization of phytoplankton and detrital absorption properties in the Sargasso Sea, Limnol. Oceanogr., 34(8), 1706–1726, 1989.

Jiang, M.-S., Chai, F., Dugdale, R. C., Wilkerson, F. P., Peng, T.-H., and Barber, R. T.: A nitrate and silicate budget in the equatorial Pacific Ocean: a coupled physical-biological model study. Deep-Sea Res. Part II, 50, 2971–2996, 2003.

Lancelot, C., Spitz, Y. H., Gypens, N., Ruddick, K., Becquevort, S., Rousseau, V., and Billen,

Bio-optical modeling

M. Fujii et al.

EGU

G.: Modelling diatom-Phaeocystis blooms and nutrient cycles in the Southern Bight of the North Sea: the MIRO model, Mar. Ecol. Prog. Ser., 289, 63–78, 2005.

Mobley, C. D. and Sundman, L. K.: Hydrolight 4.1 User's Guide (Sequoia Scientific, Inc., Redmond, Wash.), 2000a.

5 Mobley, C. D. and Sundman, L. K.: Hydrolight 4.1 Technical Documentation (Sequoia Scientific, Inc., Redmond, Wash.), 2000b.

Mobley, C. D., Sundman, L. K., and Boss, E.: Phase function effects on oceanic light fields, Appl. Opt., 41(6), 1035–1050, 2002.

Moore, J. K., Doney, S. C., Kleypas, J. A., Glover, D. M., and Fung, I. Y.: An intermediate

10 complexity marine ecosystem model for the global domain, Deep-Sea Res. Part II, 49, 403–462, 2002.

Moore, L. R., Goericke, R., and Chisholm, S. W.: Comparative physiology of Synechococcus and Prochlorococcus: influence of light and temperature on growth, pigments, fluorescence and absorptive properties, Mar. Ecol. Prog. Ser., 116, 259–275, 1995.

15 Morel, A., Optical properties of pure water and pure seawater, in: Optical Aspects of Oceanography, edited by: Jerlov, N. G. and Nielsen, E. S., Academic, New York, 1–24, 1974.

Mueller, J. L. and Lange, R. E.: Bio-optical provinces of the northeast Pacific Ocean: a provisional analysis, Limnol. Oceanogr., 34, 1572–1586, 1989.

Nakamoto, S., Kumar, S. P., Oberhuber, J. M., Muneyama, K., and Frouin, R.: Chlorophyll

20 modulation of sea surface temperature in the Arabian Sea in a mixed-layer isopycnal general circulation model, Geophys. Res. Lett., 27(6), 747–750, 2000.

Oubelkheir, K., Claustre, H., Sciandra, A., and Babin, M.: Bio-optical and biogeochemical properties of different trophic regimes in oceanic waters, Limnol. Oceanogr., 50, 1795–1809, 2005.

25 Pacanowski, R. C. and Philander, S. G. H.: Parameterization of vertical mixing in numerical models of tropical oceans, J. Phys. Oceanogr., 11, 1443–1451, 1981.

Parslow, J. S., Clementson, L. A., Turnbull, A. R., and McKenzie, D. C.: Bio-optical characteristics of oceans around Australia, in: Ocean Optics XIV Conferece Papers, vol. 1, Hawaii, November 1998 (CD-ROM).

30 Pegau, W. S.: The distribution of colored dissolved organic matter (CDOM) in the Equatorial Pacific, Ocean Optics XIII, edited by: Ackleson, S. G. and Frouin, R., 2963, 508–513, 1997.

Peña, M. A., Lewis, M. R., and Harrison, W. G.: Primary productivity and size structure of phytoplankton biomass on a transect of the equator at 135° W in the Pacific Ocean, Deep-

BGD

4, 1585–1631, 2007

Bio-optical modeling

M. Fujii et al.

Title Page

Abstract	Introduction
Conclusions	References
Tables	Figures

|◄   ►|

◄   ►

Back   Close

Full Screen / Esc

Printer-friendly Version

Interactive Discussion

EGU

Sea Res., 37, 295–315, 1990.

Pope, R. M. and Fry, E. S.: Absorption spectrum (280–700 nm) of pure water. II. Integrating cavity measurements, Appl. Opt., 36, 8710–8723, 1997.

Riley, G. A., Stommel, H., and Bumpus, D. F.: Quantitative ecology of the plankton of the western North Atlantic, Bulletin of the Bingham Oceanographic Collection Yale University, 12, 1–169, 1949.

Roesler, C. S., Perry, M. J., and Carder, K. L.: Modeling in situ phytoplantkon absorption from total absorption spectra in productive inland marine waters, Limnol. Oceanogr., 34, 1510–1523, 1989.

Rothstein, L. M., Cullen, J. J., Abbott, M., Chassignet, E. P., Denman, K., Doney, S. C., Ducklow, H., Fennel, K., Follows, M., Haidvogel, D., Hoffman, E., Karl, D. M., Kindle, J., Lima, I., Maltrud, M., McClain, C., McGillicuddy, D., Olascoaga, M. J., Spitz, Y., Wiggert, J., and Yoder, J.: Modeling ocean ecosystems – The paradigm program –, Oceanography, 19(1), 22–51, 2006.

Rudnick, D. L. and Perry, M. J.: ALPS: Autonomous and Lagrangian Platforms and Sensors, Workshop Report, 64 pp, 2003.

Schartau, M. and Oschlies, A.: Simultaneous data-based optimization of a 1D-ecosystem model at three locations in the North Atlantic: Part I – Method and parameter estimates, J. Mar. Res., 61, 765–793, 2003.

Siegel, D. A., Maritorena, S., Nelson, N. B., Hansell, D. A., and Lorenzi-Kayser, M.: Global distribution and dynamics of colored dissolved and detrital organic materials, J. Geophys. Res., 107(C12), 3228, doi:10.1029/2001JC000965, 2002.

Simeon, J., Roesler, C., Pegau, W. S., and Dupouy, C.: Sources of spatial variability in light absorbing components along an equatorial transect from 165° E to 150° W, J. Geophys. Res., 108(C10), 3333, doi:10.1029/2002JC001613, 2003.

Stramski, D., Boss, E., Bogucki, D., and Voss, K. J.: The role of seawater constituents in light backscattering in the ocean, Progress in Oceanography, 61(1), 27–55, 2004.

Stramski, D. and Kiefer, D. A.: Light scattering by microzooorganisms in the open ocean, Prog. Oceanogr., 28, 343–383, 1991.

Stramski, D., Reynolds, R. A., Kahzu, M., and Mitchell, B. G.: Estimation of particulate organic carbon in the ocean from satellite remote sensing, Science, 285(5433), 239–242, 1999.

Twardowski, M. S., Boss, E., Macdonald, J. B., Pegau, W. S., Barnard, A. H., and Zaneveld, J. R.: A model for estimating bulk refractive index from the optical backscattering ratio and the

Title Page

Abstract | Introduction

Conclusions | References

Tables | Figures

|◀ | ▶|

◀ | ▶

Back | Close

Full Screen / Esc

Printer-friendly Version

Interactive Discussion

EGU

implications for understanding particle composition in case I and case II waters, J. Geophys. Res., 106, 14 129–14 142, 2001.

Wyrtki, K.: An estimate of equatorial upwelling in the Pacific, J. Phys. Oceanogr., 11, 1205–1214, 1981.

Bio-optical modeling

M. Fujii et al.

Title Page

Abstract	Introduction
Conclusions	References
Tables	Figures

◄ ►◄

◄ ►

Back | Close

Full Screen / Esc

Printer-friendly Version

Interactive Discussion

EGU

Bio-optical modeling

M. Fujii et al.

Title Page

Abstract | Introduction

Conclusions | References

Tables | Figures

◄◄ | ►►

◄ | ►

Back | Close

Full Screen / Esc

Printer-friendly Version

Interactive Discussion

EGU

Table 1. The model parameters and values. Columns Case 1–1, Case 1–2, and Case 2 denote the parameter values used in non-spectral ecosystem model (Cases 1–1 and 1–2, without optics) and bio-optical model (Case 2), respectively.

Parameters	Symbol	Chai et al. (2002)	Case 1–1	Case 1–2	Case 2	Unit	Reference
For ecosystem model							
light attenuation coefficient due to water	k_1	0.046	0.046	0.053	N/A	m^{-1}	(1)
light attenuation coefficient by chlorophyll	k_2	0.048	0.048	0.064	N/A	$(mgChl\ m^{-3})^{-1}$	(1)
NH_4 inhibition parameter	Ψ	5.59	5.59	5.59	5.59	$(mmolN\ m^{-3})^{-1}$	(1)
Half-saturation for NO_3 uptake by picoplankton	K_{NO3}	1.0	1.0	1.0	1.0	$mmolN\ m^{-3}$	(1)
Half-saturation for NH_4 uptake by picoplankton	K_{NH4}	0.05	0.05	0.05	0.05	$mmolN\ m^{-3}$	(1)
Half-saturation for $Si(OH)_4$ uptake	$K_{Si(OH)4}$	3.0	3.0	3.0	3.0	$mmolSi\ m^{-3}$	(1)
Half-saturation for NH_4 uptake by diatoms	K_{P2_NH4}	1.0	1.0	1.0	1.0	$mmolN\ m^{-3}$	(1)
Diatom sinking speed	W_1	1.0	1.0	1.0	1.0	$m\ day^{-1}$	(1)
Microzooplankton maximum specific grazing rate	$G1_{max}$	1.35	1.6	1.35	1.35	day^{-1}	(1)
Microzooplankton assimilation efficiency	γ_0	1.0	1.0	1.0	1.0	dimensionless	(1)
Half-saturation for microzooplankton ingestion	$K1_{gr}$	0.5	0.5	0.5	0.5	$mmolN\ m^{-3}$	(1)
Microzooplankton excretion rate to NH_4	reg_1	0.2	0.2	0.2	0.2	day^{-1}	(1)
Mesozooplankton maximum specific grazing rate	$G2_{max}$	0.64	0.64	0.64	0.64	day^{-1}	(2)
Mesozooplankton assimilation efficiency	γ_1	0.75	0.75	0.75	0.75	dimensionless	(1)
Half-saturation for mesozooplankton ingestion for diatoms, microzooplankton, and NAP	$K2_{gr}$	0.25	0.25	0.25	0.25	$mmolN\ m^{-3}$	(1)
Diatom-specific mortality rate	γ_3	0.05	0.05	0.05	0.05	day^{-1}	(1)
Mesozooplankton-specific mortality rate	γ_2	0.05	0.05	0.05	0.05	day^{-1}	(1)
Mesozooplankton excretion rate to NH_4	reg_2	0.1	0.1	0.1	0.1	day^{-1}	(1)

Table 1. Continued.

Parameters	Symbol	Chai et al. (2002)	Case 1–1	Case 1–2	Case 2	Unit	Reference
Grazing preference for diatoms	ρ_1	0.7	0.7	0.7	0.7	dimensionless	(1)
Grazing preference for microzooplankton	ρ_2	0.2	0.2	0.2	0.2	dimensionless	(1)
Grazing preference for NAP	ρ_3	0.1	0.1	0.1	0.1	dimensionless	(1)
NAP remineralization rate	γ_7	0.0	0.0	0.0	0.0	day^{-1}	(1)
bSiO$_2$ dissolution rate	γ_4	0.0	0.0	0.0	0.0	day^{-1}	(1)
NAP sinking speed	W_2	10.0	10.0	10.0	10.0	m day^{-1}	(1)
bSiO$_2$ sinking speed	W_4	20.0	20.0	20.0	20.0	m day^{-1}	(1)
Diatom Si:N uptake ratio	R_{SiN}	1.0	1.0	1.0	1.0	molSi (molN)$^{-1}$	(1)
Nitrification rate	γ_5	0.0	0.0	0.0	0.0	day^{-1}	(1)
Ratio of carbon to nitrogen in phytoplankton	R_{CN}	6.625	6.625	6.625	6.625	molC (molN)$^{-1}$	(1)
For photo-acclimation model							
Chlorophyll-specific initial slope of P vs. I curve for phytoplankton	α	N/A	0.25	0.25	0.25	molC m^2 (gChl W day)$^{-1}$	(3)
Minimum phytoplankton nitrogen:carbon ratio	Q_{min}	N/A	0.034	0.034	0.034	molN molC^{-1}	(4)
Maximum phytoplankton nitrogen:carbon ratio	Q_{max}	N/A	0.17	0.17	0.17	molN molC^{-1}	(4)
Maximum picoplankton carbon-specific nitrogen-uptake rate at temperature T_{ref}	P_{ref}^{C1}	N/A	2.0	2.0	2.0	day^{-1}	(3)
Maximum diatom carbon-specific nitrogen-uptake rate at temperature T_{ref}	P_{ref}^{C2}	N/A	3.0	3.0	3.0	day^{-1}	(3)
Maximum value of θ^N	θ_{max}^N	N/A	4.2	4.2	4.2	gChl molN^{-1}	(4)
Cost of biosynthesis	ζ_{NO3}	N/A	2.33	2.33	2.33	molC molN^{-1}	(4)
Slope of an Arrehenius plot	Ea/R	N/A	−4000	−4000	−4000	K	(3)
Reference temperature	T_{ref}	N/A	303.15	303.15	303.15	K	(3)
For optical model							
Minimum phytoplankton chlorophyll to carbon ratio	θ_{min}^C	N/A	N/A	N/A	0.036	mgChl mmolC^{-1}	(5),(6),(7)
Maximum phytoplankton chlorophyll to carbon ratio	θ_{max}^C	N/A	N/A	N/A	1.2	mgChl mmolC^{-1}	(5),(6),(7)
Carbon-specific absorption coefficient by NAP at 440 nm	$a_{NAP}^+(440)$	N/A	N/A	N/A	0.1	m^2 gC^{-1}	(8),(9)

Title Page

Abstract | Introduction

Conclusions | References

Tables | Figures

◀◀ | ▶▶

◀ | ▶

Back | Close

Full Screen / Esc

Printer-friendly Version

Interactive Discussion

EGU

Table 1. Continued.

Parameters	Symbol	Chai et al. (2002)	Case 1–1	Case 1–2	Case 2	Unit	Reference
Absorption coefficient by CDOM at 440 nm	$a_{CDOM}(440)$	N/A	N/A	N/A	0.016	m^{-1}	(10)
Background backscattering coefficient	b_{bbg}	N/A	N/A	N/A	0.00017	m^{-1}	(11)
Ratio of phytoplankton carbon to POC	R_{POC}^{ϕ}	N/A	N/A	N/A	0.3	dimensionless	(12),(13),(14),(15)
Backscattering ratio for picoplankton	$\tilde{b}_{b\_P1}$	N/A	N/A	N/A	0.01	dimensionless	(16)
Backscattering ratio for diatoms	$\tilde{b}_{b\_P2}$	N/A	N/A	N/A	0.006	dimensionless	(17),(18)
Backscattering ratio for NAP	$\tilde{b}_{b\_NAP}$	N/A	N/A	N/A	0.015	dimensionless	(16)
Backscattering ratio for background particles	$\tilde{b}_{b\_bg}$	N/A	N/A	N/A	0.02	dimensionless	(16)
Backscattering ratio for sea water	$\tilde{b}_{b\_sw}$	N/A	N/A	N/A	0.5	dimensionless	(18)

References noted here are: (1) Chai et al. (2002); (2) this study; (3) Moore et al. (2002); (4) Geider et al. (1998); (5) Falkowski et al. (1985); (6) Geider et al. (1987); (7) Cloern et al. (1995); (8) Babin et al. (2003a); (9) Babin et al. (2003b); (10) Simeon et al. (2003); (11) Behrenfeld and Boss (2006); (12) Eppley et al. (1992); (13) DuRand et al. (2001); (14) Gundersen et al. (2001); (15) Oubelkheir et al. (2001); (16) Twardowski et al. (2001); (17) Boss et al. (2004); (18) Morel (1974).

Table 2. Sensitivity of model results to optical parameters: Carbon-specific absorption coefficient by NAP at 440 nm ($a^+_{NAP}(440)$), absorption coefficient by CDOM at 440 nm ($a_{CDOM}(440)$), background backscattering coefficient (b_{bbg}), ratio of phytoplankton carbon to POC (R^ϕ_{POC}), backscattering ratio for picoplankton ($\tilde{b}_{b\_P1}$), diatoms ($\tilde{b}_{b\_P2}$), NAP ($\tilde{b}_{b\_NAP}$), and background particles ($\tilde{b}_{b\_bg}$). Values in parentheses denote model results from a control run with bio-optical model. Euphotic layer depth is defined as a depth of 0.1% of sea surface.

Parameter	Observed values	Value for sensitivity study	Surface NO_3 (mmolN m^{-3}) (6.6)	Surface $Si(OH)_4$ (mmolSi m^{-3}) (2.2)	Maximum chlorophyll (mgChlm^{-3}) (0.34)	Depth of maximum chlorophyll (m) (50)	Mean $a_{NAP}/a_p(440)$ above 100 m (0.15)	Mean C_p (660) above 100 m (m^{-1}) (0.069)	Euphotic layer depth (m) (115)
$a^+_{NAP}(440)$	0.1[1]	0.07–0.13 (0.1)	6.4–6.7	2.0–2.3	0.33–0.35	50	0.10–0.20	0.068–0.070	115
$a_{CDOM}(440)$	0.012–0.025[2]	0.011–0.021 (0.016)	5.7–7.1	1.7–2.9	0.31–0.38	60–85	0.14–0.17	0.066–0.072	110–120
$\tilde{b}_{b\_bg}$	0.00017[3]	0.00012–0.00022 (0.00017)	6.6	2.1–2.2	0.34	60	0.15	0.066–0.071	115
R^ϕ_{POC}	0.25–0.4[4]	0.21–0.39 (0.3)	6.5–6.7	2.1–2.2	0.34	50–55	0.15	0.059–0.086	115
$\tilde{b}_{b\_P1}$	0.01–0.013[5]	0.007–0.013 (0.01)	6.6	2.2	0.34	50	0.15	0.065–0.076	115
$\tilde{b}_{b\_P2}$	0.006–0.007[6]	0.004–0.008 (0.006)	6.6	2.2	0.34	50	0.15	0.067–0.073	115
$\tilde{b}_{b\_NAP}$	0.015–0.02[5]	0.011–0.020 (0.015)	6.6	2.2	0.34	50	0.15	0.061–0.083	115
$\tilde{b}_{b\_bg}$	0.02[5]	0.014–0.026 (0.02)	6.6	2.2	0.34	50	0.15	0.067–0.073	115

Sources noted here are: (1) Babin et al. (2003a, b); (2) Simeon et al. (2003); (3) Stramski and Kiefer (1991), Cho and Azam (1990), and Behrenfeld and Boss (2006); (4) Eppley et al. (1992), DuRand et al. (2001), Gundersen et al. (2001), and Oubelkheir et al. (2005); (5) Twardowski et al. (2001); (6) Twardowski et al. (2001), and Boss et al. (2004).

EGU
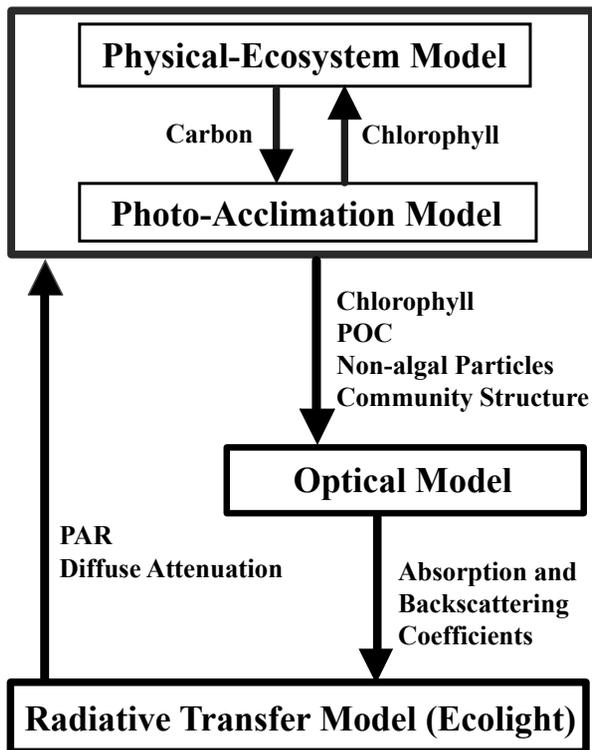
Fig. 1. Schematic view of model used in this study.

EGU
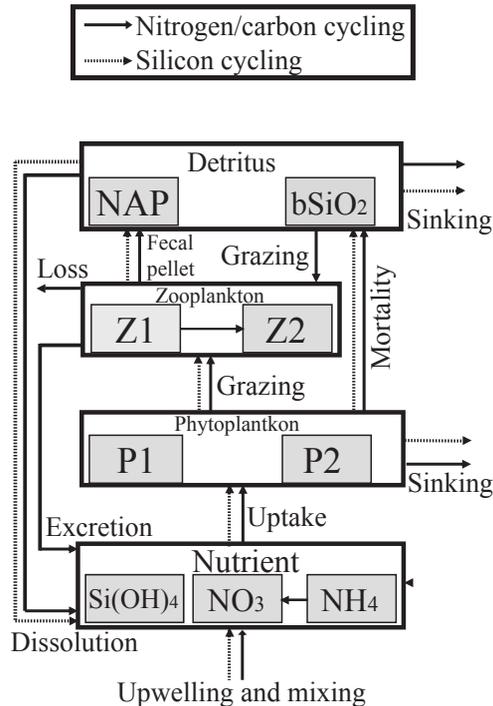
Fig. 2. The inter-compartmental flow chart of the ecosystem and linkage to physical processes. The flows of nitrogen and silicon are indicated by solid and dashed lines, respectively. P1: picoplankton (mmolN m^{-3}), P2: diatoms (mmolN m^{-3}), Z1: microzooplankon (mmolN m^{-3}), Z2: mesozooplankton (mmolN m^{-3}), NO$_3$: nitrate (mmolN m^{-3}), NH$_4$: ammonium (mmolN m^{-3}), Si(OH)$_4$: silicate (mmolSi m^{-3}), NAP: non-algal particles (mmolN m^{-3}), and bSiO$_2$: biogenic silica (mmolSi m^{-3}).
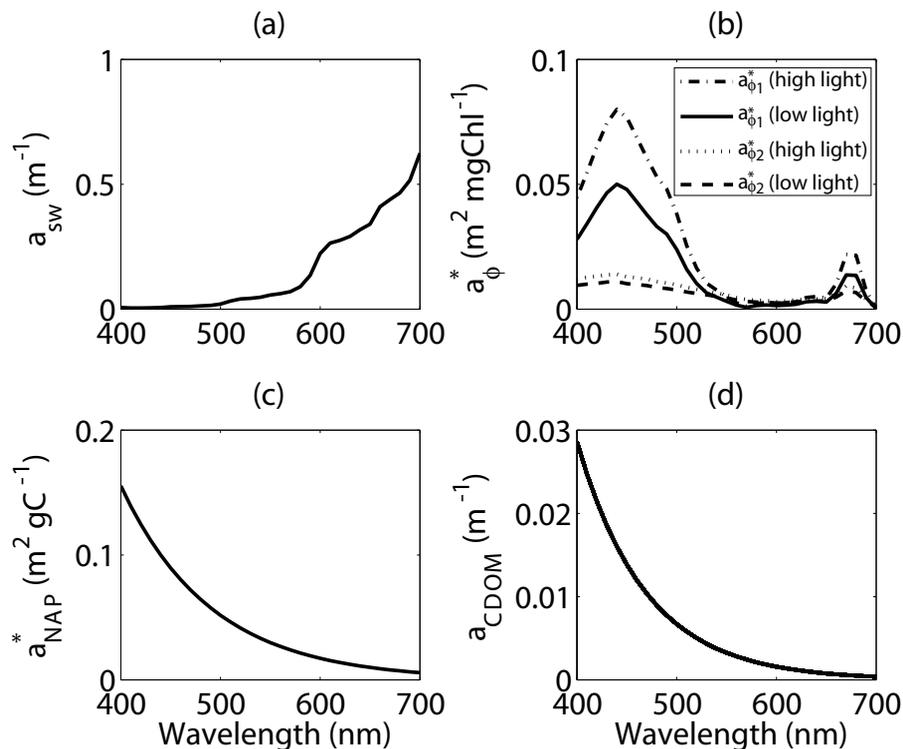
Fig. 3. Modeled **(a)** absorption coefficient by sea water a_{sw} (m^{-1}), **(b)** chlorophyll-specific absorption coefficients by picoplankton and diatoms ($a_{\phi 1}^{*}$ and $a_{\phi 2}^{*}$, respectively) (m^2 mgChl^{-1}), **(c)** carbon-specific absorption coefficient by NAP (m^2 gC^{-1}), and **(d)** absorption coefficient by CDOM (m^{-1}) from 400 nm to 700 nm.

EGU

EGU

(a)

(b)
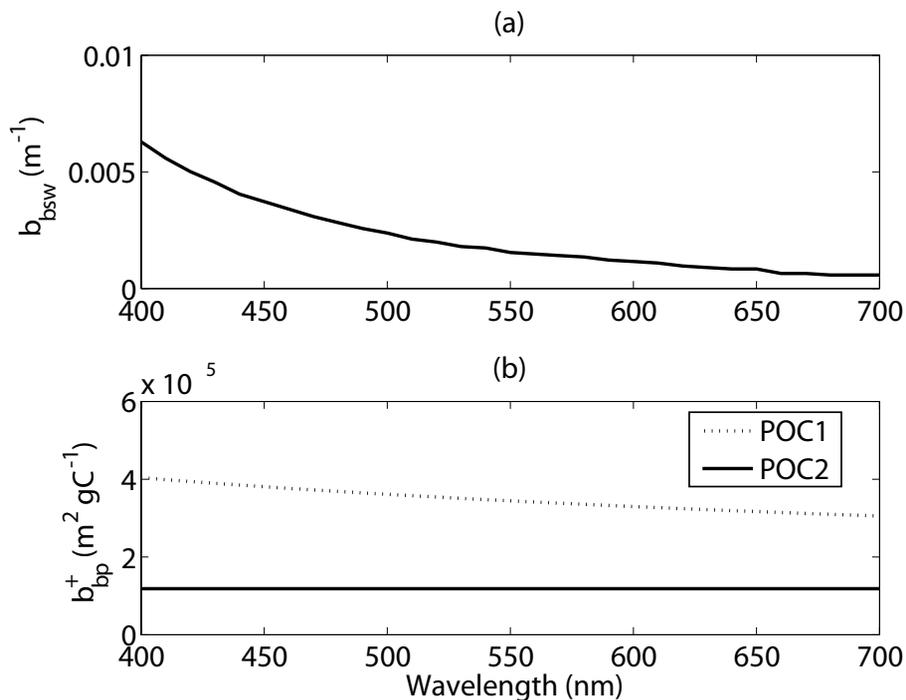
Fig. 4. Modeled **(a)** backscattering coefficient by sea water b_{bsw} (m^{-1}) and **(b)** carbon-specific backscattering coefficients b_{bp}^{+} by small POC (POC1) and large POC (POC2) from 400 nm to 700 nm.
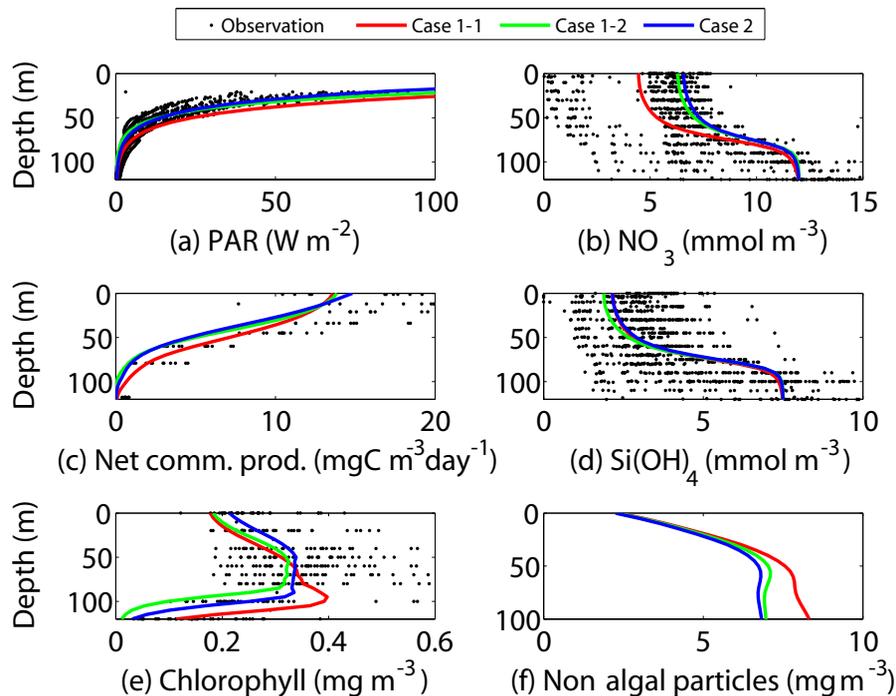
Fig. 5. Modeled vertical profile of **(a)** PAR ($W\,m^{-2}$), **(b)** NO_3 ($mmolN\,m^{-3}$), **(c)** net community production ($mgC\,m^{-3}\,day^{-1}$), **(d)** $Si(OH)_4$ ($mmolSi\,m^{-3}$), **(e)** chlorophyll ($mgChl\,m^{-3}$), and **(f)** non-algal particles NAP ($mgC\,m^{-3}$) in Cases 1–1 (without optics), 1–2 (without optics), and 2 (with optics). Dots denote the U.S. JGOFS EqPac data for TT011 and TT012.

EGU
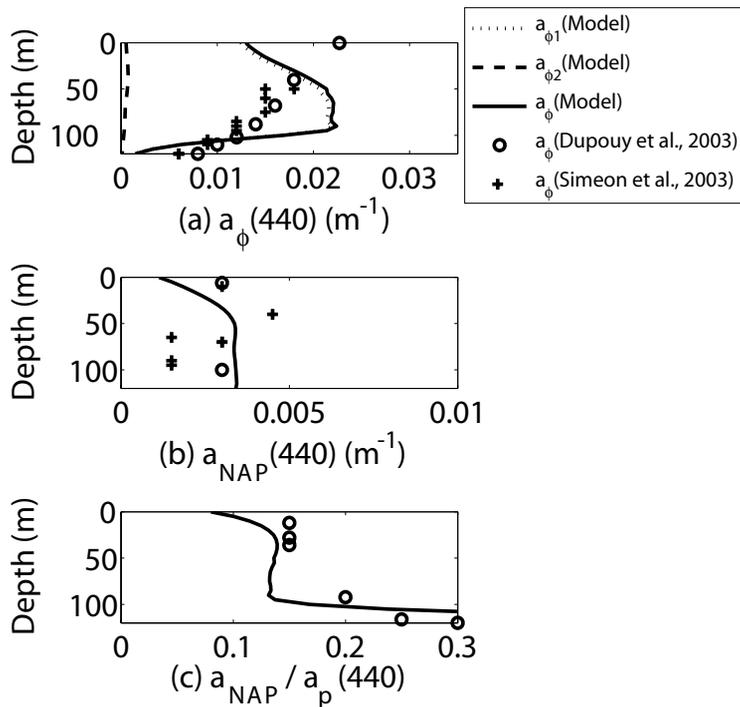
Fig. 6. Modeled vertical profile of **(a)** absorption coefficients at 440 nm by picoplankton P1 ($a_{\phi 1}(440)$), diatoms P2 ($a_{\phi 2}(440)$), and total phytoplankton (P1+P2) ($a_{\phi}(440)$) (m^{-1}), **(b)** absorption coefficient at 440 nm by non-algal particles NAP ($a_{NAP}(440)$) (m^{-1}), and **(c)** ratio of NAP absorption to total particle absorption at 440 nm ($a_{NAP} / a_{P}(440)$).

EGU
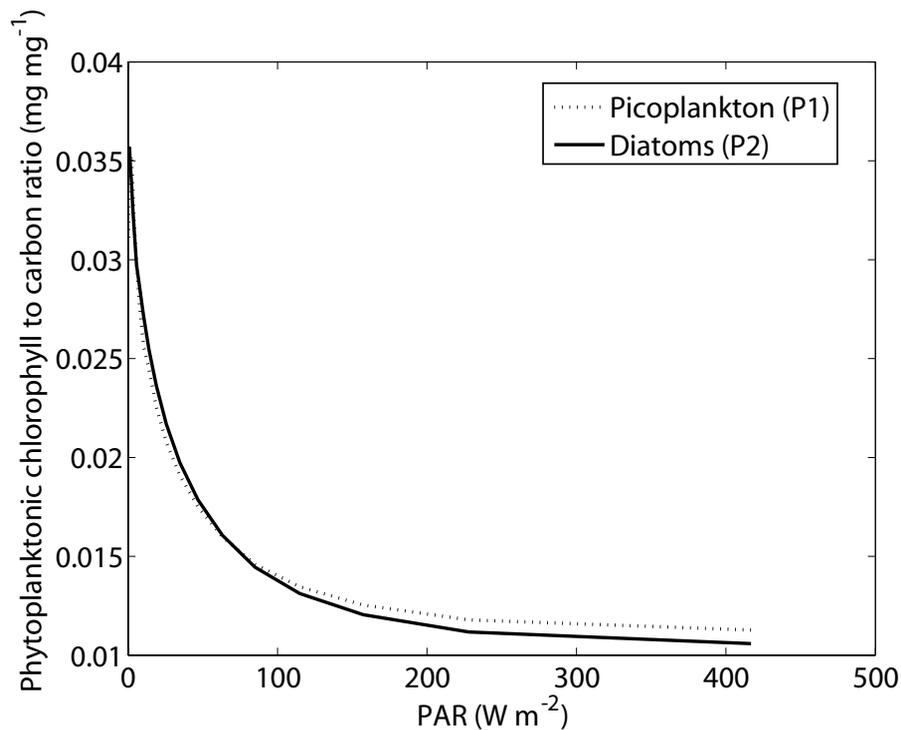
Fig. 7. Modeled phytoplanktonic chlorophyll to carbon ratio ($mg\,mg^{-1}$) versus PAR ($W\,m^{-2}$) by picoplankton P1 and diatoms P2.

EGU
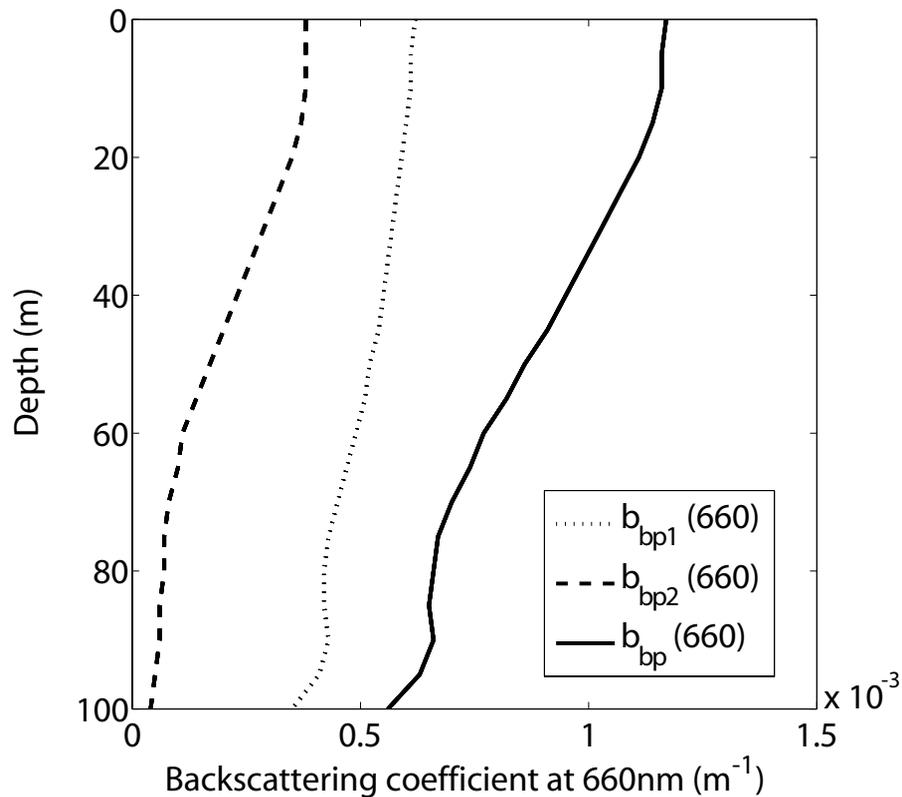
Fig. 8. Modeled vertical profile of backscattering coefficients at 660 nm by small POC (POC1) ($b_{bp1}(660)$), large POC (POC2) ($b_{bp2}(660)$), and total POC (POC1+POC2) ($b_{bp}(660)$) (m^{-1}).

EGU
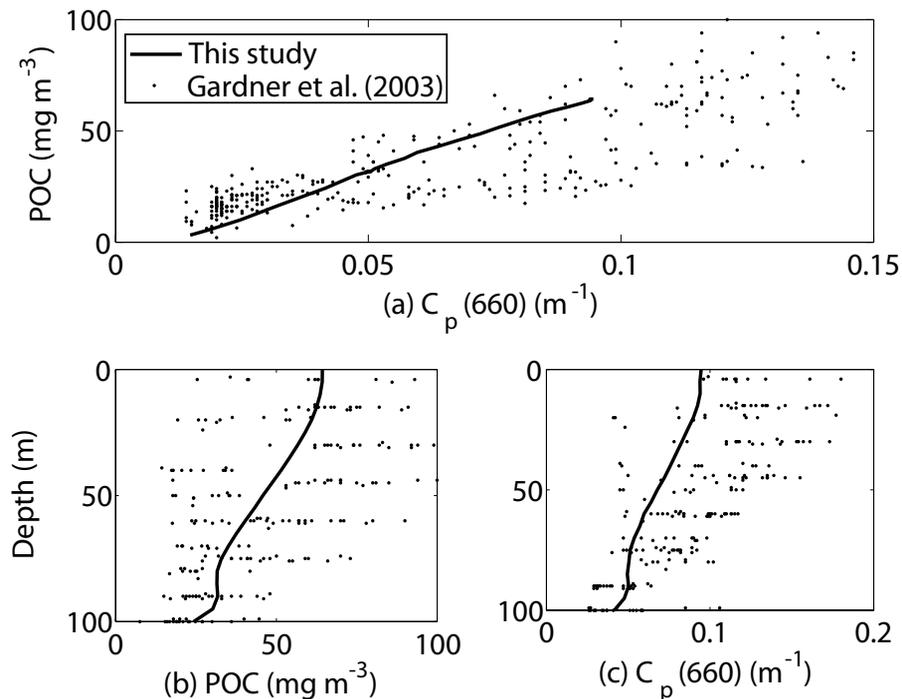
Fig. 9. Modeled vertical profile of **(a)** POC (mg m^{-3}) and **(b)** beam attenuation coefficient by particles at 660 nm ($C_p(660)$) (m^{-1}). Dots denote the U.S. JGOFS EqPac data for TT011 and TT012 (Gardner et al., 2003).